November 9–14, 2026
Ljubljana, Slovenia

Proceedings of the

Electroporation-Based Technologies and Treatments

20th International SCIENTIFIC WORKSHOP and POSTGRADUATE COURSE

Edited by:

Saša Haberl Meglič
Damijan Miklavčič

2026

Organized by:

UNIVERZA V LJUBLJANI
University of Ljubljana

ONKOLOŠKI INŠTITUT
INSTITUTE OF ONCOLOGY
LJUBLJANA

Supported by:

Abbott

ArgaMedtech
NEXT GENERATION CARDIAC ABLATION

BES
The Bioelectrochemical Society

Boston Scientific

CARDIO FOCUS

COBIK

elea

Field MEDICAL

IGEA
CLINICAL BIOPHYSICS

imricor

ION OPTIX

ISEBTT International Society for Electroporation-Based Technologies and Treatments

IskraMedical

IVY BIOMEDICAL

Johnson&Johnson MedTech

Kardium

ELECTROvet EZ
by LEROY BIOTECH

LIFE PULSE

Medtronic

MIRAI MEDICAL

mpor

omega

pio
Clean visions.

Pulse Biosciences

VITAVE

November 9-14, 2026

Ljubljana, Slovenia

Proceedings of the

Electroporation-Based Technologies and Treatments

20th International SCIENTIFIC WORKSHOP and POSTGRADUATE COURSE

Edited by:
Saša Haberl Meglič
Damijan Miklavčič

Organized by:

University of Ljubljana,
Faculty of Electrical Engineering

Institute of Oncology, Ljubljana

Supported by:

Bioelectrochemical Society

International Society for Electroporation-Based Technologies and Treatments

Organising committee

Chair:

Saša Haberl Meglič

Members:

Lana Balentović, Anja Blažič, Klara Bulc-Rozman, Helena Cindrič, Duša Hodžić, Barbara Ž. B. Gantar, Jernej Jurič, Samo Mahnič, Urša Primožič, Rok Šmerc, Zala Vidic, Angelika Vižintin

Abbott
ArgaMedtech
Boston scientific
CardioFocus
COBIK
ELEA
Field Medical
IGEA
Imricor Medical Systems
IonOptix
Iskra Medical
Iskra PIO
Ivy Biomedical Systems
Johnson&Johnson Medtech
Kardium
Leroy Biotech
LifePulse Corp.
Medtronic
Mirai Medical
mPOR
OMEGA
Pulse Biosciences
VITAVE Tech

www.ebtt.org

Kataložni zapis o publikaciji (CIP) pripravili v Narodni in univerzitetni knjižnici v Ljubljani

COBISS.SI-ID 303685891

ISBN 978-961-243-506-6 (PDF)

URL: https://2026.ebtt.org/

Copyright © 2026 Založba FE. All rights reserved. Razmnoževanje (tudi fotokopiranje) dela v celoti ali po delih brez predhodnega dovoljenja Založbe FE prepovedano.

Naslov: Proceedings of the Electroporation-based Technologies and Treatments

Založnik: Založba FE, Ljubljana
Izdajatelj: Fakuleta za elektrotehniko, Ljubljana
Urednik: prof. dr. Sašo Tomažič
Kraj in leto izida: Ljubljana, 2026
1. elektronska izdaja

Table of contents

Welcome note....5

INVITED LECTURERS AND NEW FACULTY MEMBERS....7

On the origin of bubbles in PFA....9

Blood is not water: hemolysis, bubble formation, protein denaturation, and hemostatic changes during pulsed field ablation....10

How PFA will change cardiac arrhythmia treatment....11

Electric field effects on proteins: direct and indirect pathways....12

Cardiac MRI characterization of lesion pathophysiology and....13

temporal evolution following pulsed field ablation....13

Collateral effects of electroporation: heating, electrical stimulation, and electrochemical reactions....14

Fundamental principles of designing safe, effective, and usable systems for cardiac ablation via pulsed electric fields....15

Irreversible electroporation as an ablation technique....16

Atrial fibrillation from genes to therapeutics....17

Vascular effects in electroporation-based treatments....18

RNA therapies for cardiac repair and regeneration....19

Irreversible electroporation for the use of cardiac ablation....20

It begins at the end - how clinical goals and constraints affect electroporation device development....21

SHORT PRESENTATIONS BY STUDENTS AND PARTICIPANTS....22

Live cell imaging and microdosimetry assessment of electroporation: an integrated in vitro and in silico approach....24

OpenDEP: a modular open-source platform for population or single-cell dielectrophoretic characterization of cells....25

Breaking the bone barrier: electrochemotherapy for bone tumours in dogs and cats, a review....26

Pulsed electric field–induced hemolysis in human blood ex vivo....27

Electric field distribution in a full porcine torso geometry with varying return electrode placement in cardiac PFA: a computational model....28

Integrated dielectrophoresis and optical tweezers for single-cell characterization....29

Electric field strength shifts protein responses from thermal-state dependence toward structure-guided remodeling....30

Annexin A4 relocalisation and plasma membrane stabilisation in response to electroporation....31

Mathematical modeling of the membrane of a cell using the Cahn Hilliard PDE....32

Effect of specific energy input on pilot-scale PEF inactivation and post-treatment survival of a beer spoilage yeast 33

Electroporation-based sampling of live tissue for spatiotemporal omics 34

Quantitative phase imaging as an intelligent label-free approach for biophysical analysis of cells and tissues 35

Computational analysis of peripheral nerve electroporation: fiber-type vulnerability and electric field effects 36

NanoediT: nanoneedle-mediated genomic editing for hypoimmunogenic regulatory T cell manufacturing.....37

Beyond bleomycin: alternative drugs for electrochemotherapy, a review 38

Cell-specific responses to patterned bipolar pulses for gene electrotransfer 39

Charge-neutral bursts of asymmetric microsecond pulses for in vivo DNA delivery 40

Response of patient-derived glioblastoma stem and differentiated cell spheroids to high-frequency biphasic electric pulses 41

In silico modeling of multicellular tumor spheroids for the optimization of DNA vaccine electroporation 42

Calcium-dependent electroporation responses: cytotoxicity, tumor suppression and annexin A4 membrane repair 43

Evaluation of circulating tumor cell dynamics following electroporation or electrochemotherapy in a 4T1 mouse model of metastatic breast cancer.....44

Therapeutic role of bleomycin-based electrochemotherapy in the treatment of locally advanced- and recurrent vulva carcinomas.....45

Electrochemotherapy for the treatment of perianal carcinoma concomitant with cervical cancer 46

Neoadjuvant, ECT-integrated surgery, and adjuvant chemotherapy for canine metastatic mast cell tumor 47

Faculty members 48

Welcome note

Dear Colleagues, dear Participants, dear Students,

The Workshop and Postgraduate Course on Electroporation-Based Technologies and Treatments (EBTT) at the University of Ljubljana was organised for the first time in 2003. In more than twenty years, over 1100 participants from 46 different countries have attended the school. And also this year we can say with great pleasure: "with the participation of many of the world's leading experts in the field". However, the aims and objectives of the school remain unchanged: to provide participants with sufficient theoretical background knowledge and practical skills to enable them to use electroporation effectively in their working environment.

It is a great pleasure to welcome you to the EBTT organised by the University of Ljubljana and the Institute of Oncology Ljubljana, which takes place at the Faculty of Electrical Engineering as an integral part of the Interdisciplinary doctoral programme Biomedicine of the University of Ljubljana. From the very beginning, we were aiming to prepare lab work for the participants that would complement the lectures. Since the preparation of lab work takes more time than the preparation and organisation of lectures, we introduced lab work at the second workshop in 2005. The lab work covers different aspects of research: biological experiments in the cell culture labs, microbiology lab, tissue lab; numerical and molecular dynamics modelling, development of pulse generators and electrical measurements using the electronic lab workshop.

After the experience of 2020, when we organized the school completely online due to the pandemic, we decided to continue organizing the course as a hybrid course to enable participation even for those who still have difficulties with travel or suffer from a lack of time. The team here in Ljubljana will therefore offer both practical lab work on site and live webinars on the lab work so that you can benefit the most even if you are not in the lab. The biological experiments were pre-recorded and will be organized in the Infrastructural Centre "Cellular Electrical Engineering", part of the University of Ljubljana's network of research and infrastructure centres, in the Laboratory of Biocybernetics. Lab works would not be possible without the extensive participation and commitment of numerous members of the Laboratory of Biocybernetics, for which I would like to thank them all cordially.

It also needs to be emphasized that all written contributions included in the proceedings were thoroughly reviewed and subsequently edited. We would like to thank all authors and reviewers for their diligent work. I would also like to express our sincere gratitude to the faculty members and invited lecturers for their lectures delivered at the course. Finally, I would like to thank our sponsors as well as the Bioelectrochemical Society and the International Society for Electroporation-Based Technologies and Treatments for supporting us and making our EBTT possible.

I sincerely hope you will enjoy the experience, benefit from being with us and expand your professional network.

Sincerely Yours,

Damijan Miklavčič



INVITED LECTURERS AND NEW FACULTY MEMBERS

On the origin of bubbles in PFA

Samo Mahnič[1], Damijan Miklavčič[1], Peter Lombergar[1], Blaž Mikuž[2], Lars M. Mattison[3], Daniel C. Sigg[3], Bor Kos[1]; *[1]University of Ljubljana, Faculty of Electrical Engineering, Ljubljana, SLOVENIA; [2]Jožef Stefan Institute, Reactor Engineering Division, Ljubljana, SLOVENIA; [3]Medtronic, Mounds View, USA*

INTRODUCTION

Bubble formation during pulsed field ablation (PFA) raises concerns about embolic risk. Three main mechanisms of their origin are proposed: boiling [1,5], electrolysis [2,3], and degassing [3,4]. Distinguishing between them is essential to improve safety and optimize ablation protocols.

MATERIALS AND METHODS

Experiments were performed in saline using a modified RF ablation catheter. Monophasic and biphasic pulse protocols were delivered, while bubble dynamics were recorded with a 10,000 fps high-speed camera. Numerical simulations of electric and thermal fields were performed in COMSOL Multiphysics to identify hotspots.

RESULTS AND DISCUSSION

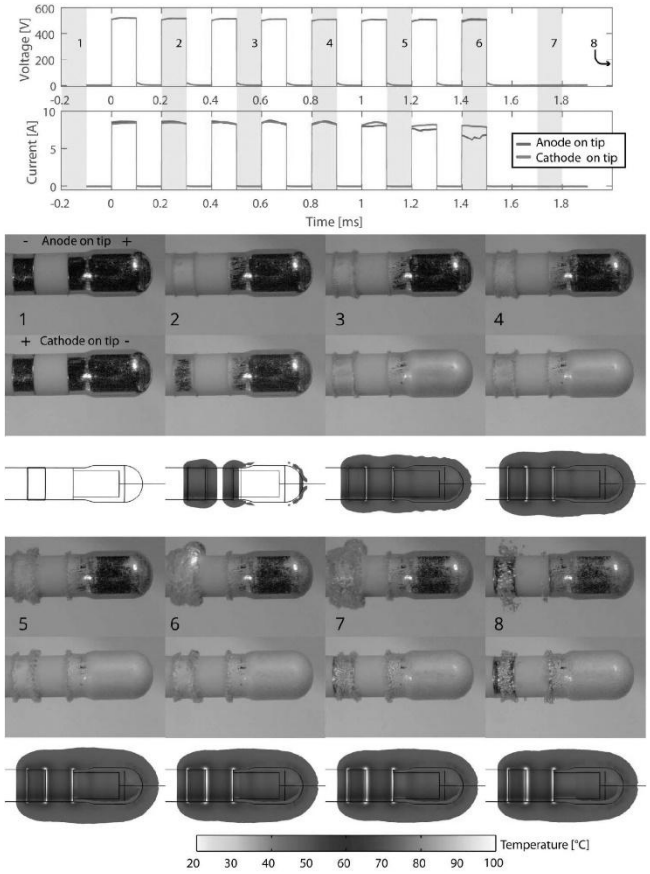


Figure 1: Delivery of monophasic (100 µs, 5 kHz, n = 8, train duration 1.5 ms) pulses between the catheter tip and ring electrodes – high-speed camera images and numerical simulations of heating.

High-speed imaging showed that monophasic pulses produced stable, persistent bubbles consistent with electrolysis, whereas biphasic pulses generated transient vapor bubbles that quickly collapsed.

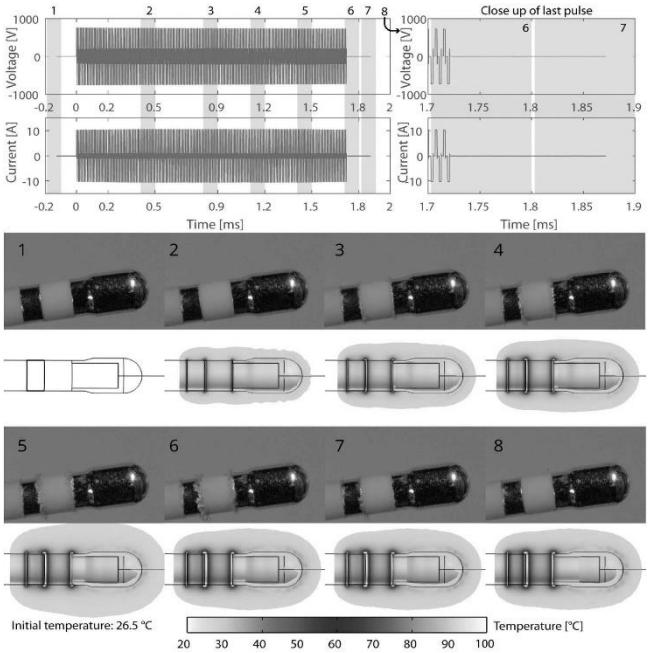


Figure 2: Delivery of biphasic pulses (2-2-2-2 µs, n = 216, train duration 1.73 ms) imaged by the high-speed camera, with corresponding numerical simulations of heating.

Modelling confirmed hotspots near electrode edges coinciding with boiling onset, while electrolysis-driven bubbles originated from and persisted due to electrode reactions. Degassing, though contributing a smaller gas volume than boiling or electrolysis, can still generate long-lived bubbles, which may persist in the bloodstream.

CONCLUSIONS

Electrolysis dominates bubble formation in monophasic PFA, while biphasic pulses primarily induce transient boiling. Protocols with short biphasic pulses and optimized geometry minimize bubble generation and improve safety.

REFERENCES

[1] Verma A., *et al. Circ Arrhythm Electrophysiol*, 14, 2021.
[2] Aycock K.N., *et al. Bioelectricity*, 1:214-234, 2019.
[3] van Es R., *et al. J Cardiovasc Electrophysiol*, 30:2071-2079, 2019.
[4] Campana L. G., *et al. Eur J Surg Oncol*, 45:92–102, 2019.
[5] Reddy V.Y., *et al. N Engl J Med*, 389:1660-1671, 2023.

Blood is not water: hemolysis, bubble formation, protein denaturation, and hemostatic changes during pulsed field ablation

Katarina Reberšek[1], Marko Žavbi[2], Tamara Polajžer[3], Martina Fink[1], Nejc Špendal[2], Darko Černe[1], Damijan Miklavčič[3], Matej Reberšek[3]; *[1]Department of Hematology, University Medical Centre Ljubljana, Ljubljana, SLOVENIA; [2]Clinical Institute for Clinical Chemistry and Biochemistry, University Medical Centre Ljubljana, Ljubljana, SLOVENIA; [3]University of Ljubljana, Faculty of Electrical Engineering, Ljubljana, SLOVENIA*

INTRODUCTION

Pulsed field ablation (PFA) produces cardiac ablation primarily by irreversible electroporation and is therefore regarded as predominantly non-thermal. However, blood adjacent to catheter electrodes may experience high electric fields, substantial cumulative pulse energy, and marked local heating. Clinical PFA has been associated with intravascular hemolysis [1], microbubble formation, and thromboembolic events, while significant hemolysis has also been demonstrated during irreversible electroporation of cardiomyocytes in vitro [2]. We investigated how blood composition modifies the response to high-intensity PFA, focusing on hemolysis, gas-bubble formation, protein denaturation, and hemostasis.

METHODS

Exploratory static in vitro experiments used human whole blood, plasma, concentrated erythrocytes, half-saline, and control serum. Samples received 800-2000 biphasic pulses at 500-2500 V/cm; concentrated erythrocytes were additionally studied at 4000 V/cm to compensate for low conductivity. Voltage, current, and temperature were characterized, and transient conductivity reductions detected bubble-related obstructions. Complete blood counts and plasma hemoglobin assessed erythrocyte injury and hemolysis. Time-resolved microscopy, blood oxygen partial pressure, plasma total carbon dioxide and chloride, protein assays, fibrinogen and von Willebrand factor measurements, and rotational thromboelastometry were combined with precooling, duty-cycle modification, and thermal controls to distinguish electrical from temperature-dependent effects.

RESULTS

No relevant hematological changes were observed up to 1000 V/cm. Erythrocyte injury appeared at 1500 V/cm, with increased red cell distribution width, mean corpuscular volume, and plasma hemoglobin and reduced erythrocyte count. Injury progressed at 2000 V/cm and complete hemolysis occurred at 2500 V/cm. At 2000 V/cm, precooling reduced peak temperature from approximately 71°C to 54°C and markedly attenuated erythrocyte damage, suggesting dominant role of thermal injury. Nevertheless, microscopy identified early membrane blebbing during high-field PFA at approximately 33°C; which was not reproduced by low-voltage sinusoidal heating, indicating an electric-field effect. Later spherical transformation, vesiculation, intracellular optical changes, bubble release, and hemolysis were reproduced by heating controls and were predominantly heat driven.

Bubble formation depended strongly on sample composition. The first bubble-related signal appeared at approximately 61°C in plasma and whole blood, compared with approximately 73°C in half-saline, while concentrated erythrocytes showed a major bubble event at approximately 70-77°C, overlapping the reported temperature range of hemoglobin thermal denaturation [3]. Whole blood subsequently developed persistent electrode-associated plaque. PFA substantially decreased whole-blood oxygen partial pressure at 2000 and 2500 V/cm, consistent with an erythrocyte-associated process involving the oxygen pool, although bubble composition was not directly measured. Plasma total carbon dioxide and chloride were unchanged immediately after PFA, whereas 10-min thermal exposure reduced plasma total carbon dioxide above approximately 55°C, supporting temperature-dependent carbon dioxide loss as a possible plasma-related mechanism. High-field PFA and thermal exposure also reduced the detectability of several protein analytes, most prominently creatine kinase-MB. Fibrinogen concentration and von Willebrand factor activity decreased, rotational thromboelastometry showed progressive impairment of clot formation, and measurable clot formation was absent at 2500 V/cm.

CONCLUSIONS

Under static high-intensity PFA conditions, PFA-induced blood injury reflects interacting electric-field and thermal effects that cannot be adequately inferred from saline experiments alone. High PFA exposure can produce hemolysis, composition-dependent bubble formation, protein denaturation, impaired hemostasis, and electrode-associated deposits. These findings provide mechanistic framework for understanding blood-related observations during PFA, but the gas composition, thrombogenicity of the observed material. Relevance for clinically realistic waveforms in flowing blood require further investigation.

REFERENCES

[1] Popa M. A., *et al.* Characterization and clinical significance of hemolysis after pulsed field ablation for atrial fibrillation: results of a multicenter analysis. *Circ Arrhythm Electrophysiol*, 17:e012732, 2024.

[2] Fišerová I., *et al.* Significant hemolysis is present during irreversible electroporation of cardiomyocytes in vitro. *Heart Rhythm*, 22:466-474, 2025.

[3] Michnik A., *et al.* Differential scanning microcalorimetry study of the thermal denaturation of haemoglobin. *Biophys Chem*, 118:93-101, 2005.

How PFA will change cardiac arrhythmia treatment

Helmut Pürerfellner; *Department of Cardiology, Ordensklinikum Linz Elisabethinen, Linz, Austria; European Heart Rhythm Association (EHRA)*

INTRODUCTION

Pulsed field ablation (PFA) has moved cardiac ablation from thermally mediated tissue destruction towards field-controlled electroporation. This is not simply a new catheter or energy source, but a change in the therapeutic concept: myocardial cell death can be created rapidly while reducing dependence on conductive heating or freezing and, in appropriate settings, limiting injury to adjacent structures such as the oesophagus, phrenic nerve, pulmonary veins and coronary vasculature. The first and most visible consequence has been in atrial fibrillation (AF), where pulmonary vein isolation is becoming faster, more reproducible and easier to standardize.

PRESENT IMPACT

In current practice, PFA changes AF ablation in four ways. First, it improves the safety narrative of AF ablation by reducing several feared complications of thermal energy, although vigilance for technology-specific events such as vascular complications, coronary spasm or haemolysis remains mandatory. Second, it changes workflow: shorter energy delivery, less catheter instability penalty and simplified lesion deployment allow more predictable procedure duration, new sedation strategies and potentially more same-day discharge pathways. Third, it broadens access to ablation by making high-quality pulmonary vein isolation less dependent on the individual operator's thermal lesion craftsmanship. Fourth, it forces us to rethink training: future electrophysiologists must understand not only anatomy and electrograms, but also electric-field distribution, waveform design, dose, tissue contact, far-field effects and device-specific biophysics.

FUTURE DIRECTIONS

The next step will determine whether PFA remains mainly an AF pulmonary-vein technology or becomes a platform for arrhythmia treatment. Emerging applications include posterior wall ablation, mitral and cavotricuspid isthmus lines, atrial tachycardia substrates, surgical and hybrid ablation, and selected ventricular tachycardia targets. These uses will require proof that electroporation lesions are durable, transmural where needed and sufficiently selective in more complex anatomy. Imaging, including cardiac magnetic resonance, may help define acute tissue response, lesion maturation and gaps, and could become an important bridge between engineering concepts and clinical endpoints.

CONCLUSIONS

PFA will change arrhythmia treatment by shifting the field from empirical thermal lesion creation towards engineered, tissue-selective ablation. Its greatest value will not be measured only by shorter procedures, but by safer implementation, more consistent outcomes, broader patient access and better integration of biophysics, imaging and clinical electrophysiology. At the same time, PFA should not be presented as a one-size-fits-all solution. The future standard will be the intelligent selection of energy source, catheter design, lesion set and patient-specific strategy. For this reason, PFA represents both a clinical advance and a new educational responsibility for the electrophysiology community.

REFERENCES

[1] Verma A., *et al*. 2026 HRS/EHRA scientific statement on pulsed field ablation for cardiac arrhythmias. *Heart Rhythm,* 23:e2195-e2234*,* 2026.

[2] Kühne M., *et al*. Pulsed field ablation for the interventional treatment of atrial fibrillation. *Europace,* 28 : euag080, 2026.

[3] Ekanem E., *et al*. Multi-national survey on the methods, efficacy, and safety on the post-approval clinical use of pulsed field ablation (MANIFEST-PF). *EP Europace*, 24:1256-1266, 2022.

[4] Ekanem E., *et al*. Safety of pulsed field ablation in more than 17,000 patients with atrial fibrillation in the MANIFEST-17K study. *Nat Med*, 30:2020-2029, 2024.

Electric field effects on proteins: direct and indirect pathways

Michal Cifra; *Institute of Photonics and Electronics of the Czech Academy of Sciences, Prague 18200, CZECHIA. E-mail: cifra@ufe.cz*

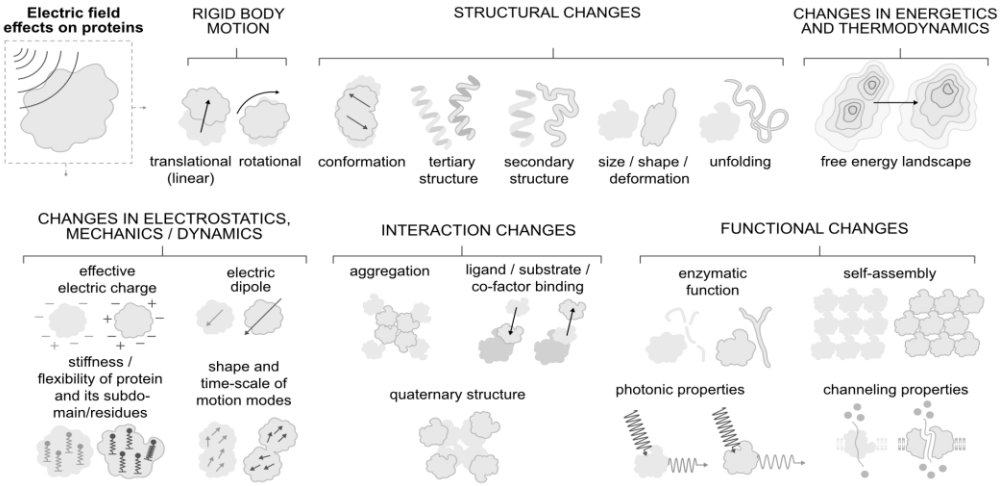


Figure 1: Overview of physical effects of an external electric field on proteins, as reported in molecular dynamics simulations and/or experiments. Adapted from [1].

INTRODUCTION

Proteins account for roughly half of the dry mass of metabolically active cells and, through catalysis, regulation and spatiotemporal organisation, underlie nearly all functions of living systems [1]. Protein activity is conventionally modulated using ligands or post-translational modifications, but an external electric field (EF) offers a complementary, physical route to the same end. By exerting a force on charged and dipolar protein groups, an EF can reshape the energetic landscape and dynamics of a protein without adding reagents, offering mass-free, rapidly switchable, non-contact control that is directly relevant to electroporation-based technologies, where the pulsed fields that permeabilize membranes inevitably also act on the proteins in and around them.

EF EFFECTS ON PROTEINS

We recently reviewed computational and experimental evidence for how EFs of different strength, waveform and duration act on proteins [1]. The EF couples directly to charged residues and dipolar groups, driving rigid-body translation and rotation and, when parameters are well tailored, cascading into changes of secondary, tertiary and quaternary structure, conformation and unfolding (Fig. 1). These structural changes are accompanied by shifts in the protein free-energy landscape, effective charge, dipole moment and mechanical stiffness, and, further downstream, in protein-protein and protein-ligand interactions and aggregation, ultimately altering protein function such as enzymatic activity, ion channelling and self-assembly.

INDIRECT EFFECTS

Not every change seen under an applied field comes from the field acting on the protein itself. In conductive media the EF also drives Joule and dielectric heating, electrohydrodynamic flows, shockwaves and cavitation, and reactive oxygen and nitrogen species [1], as well as faradaic electrode reactions that produce steep local pH shifts [2] and gas microbubbles [3]. These stresses unfold or aggregate proteins in their own right and readily mimic direct EF effects: electrode-driven pH excursions have been shown to account for apparent field-induced unfolding. Temperature and pH monitoring, radical scavengers and matched chemical controls are therefore essential before attributing a structural change to direct EF-protein coupling.

CONCLUSIONS AND OUTLOOK

Despite growing evidence for diverse and often reversible EF-driven control of proteins, the mechanisms remain only partly understood and applications have not reached their full potential [1]. Systematic reporting of EF parameters together with mechanistic, structure-based analysis is needed to turn these effects into reliable tools for biomedicine, food processing and biotechnology.

ACKNOWLEDGEMENT

This work was supported by the Czech Health Research Council (project No. NW25-08-00274) and the Czech Science Foundation (grant No. 25-16700S).

REFERENCES

[1] Cifra M., *et al*. Electric field effects on proteins: direct and indirect pathways. *Chem Soc Rev*, 2026.
[2] Šmerc R., *et al. Electrochim. Acta*, 511:145363, 2024.
[3] Mahnič-Kalamiza S., *et al. Electrochim. Acta*, 497:144550, 2024.

Cardiac MRI characterization of lesion pathophysiology and temporal evolution following pulsed field ablation

Graham A. Wright[1,2*], Terenz Escartin[1,2], Philippa R. P. Krahn[1,2]; *[1]Department of Medical Biophysics, University of Toronto, Toronto, ON, CANADA; [2]Physical Sciences Platform, Sunnybrook Research Institute, Toronto, ON, CANADA*
** Corresponding author; E-mail: gawright@sri.utoronto.ca*

INTRODUCTION

Pulsed field ablation (PFA) creates myocardial injury through nonthermal irreversible electroporation rather than the coagulative necrosis produced by radiofrequency (RF) energy [1]. Because MRI depicts the biological consequences of injury, not the injury itself, this difference is expected to alter the appearance and time-course of lesions on cardiac MRI relative to the RF paradigm, in which native T1-weighted, T2-weighted, and late gadolinium enhancement (LGE) imaging each reflect a distinct stage of thermal lesion evolution [2,3]. This presentation reviews the MRI signature of PFA lesions and its temporal evolution, to give participants a pathophysiology-based framework for interpreting post-PFA MRI.

METHODS

This review synthesizes preclinical and clinical evidence on cardiac MRI after PFA. Preclinical findings derive primarily from ventricular PFA studies in swine using focal catheters over a range of doses, imaged at 3T with native T1-weighted and 3D LGE MRI at acute (24 h), subacute (1 week), and chronic (6 week) time points, with histological validation in a subset of animals [1,4]. Additional data describe PFA in infarcted, scarred myocardium [1,4,5]. Clinical evidence comes from serial MRI before and after PFA for pulmonary vein isolation (PVI) [6-8], with an additional porcine atrial RF-versus-PFA study for direct comparison [9].

RESULTS

Native T1-weighted imaging shows little or no hyperintensity at PFA sites at any time, confirming a predominantly nonthermal injury mechanism [1]. LGE MRI provides information about lesion extent: the volume increases with dose, is maximum at the 24-hour time point, contracts significantly by 1 week, and then remains stable out to 6 weeks. The LGE-based lesion size at 6 weeks correlates closely with pathology and histology from that time point [1]. A hypoenhanced core on LGE consistent with microvascular obstruction occurs in a minority of high-dose lesions and is less extensive than after RF ablation [1]. PFA lesions extend through heterogeneous ventricular scar similarly to healthy myocardium [4,5]. Clinical atrial PFA studies show a broadly similar behavior, complicated by the thin atrial wall and by differing LGE techniques; chronic circumferential lesion coverage in PVI on LGE ranges from 12% to over 70% depending on catheter technology and segmentation threshold [6-8]. In a porcine atrial model, RF and PFA lesions of differing acute size converged to similar, smaller chronic volumes by 6 weeks [9].

CONCLUSIONS

PFA produces a distinct, nonthermal MRI signature: native T1-weighted imaging is largely uninformative, while LGE is the principal biomarker of lesion location, extent, and maturation. Early (24-hour) LGE overestimates the durable lesion, whereas subacute (~1-week) imaging is a more reliable, histologically validated predictor of chronic size. Divergent reports of chronic atrial lesion detectability likely reflect differences in ablation technology, MRI technique, and analysis methods. These principles frame MRI interpretation after PFA and its extension to ventricular applications.

REFERENCES

[1] Miklavčic D., *et al.*, Biophysics and electrophysiology of pulsed field ablation in normal and infarcted porcine cardiac ventricular tissue. *Sci Rep*, 14:32063, 2024.
[2] Dickfeld T., *et al.*, Characterization of RF ablation lesions with gadolinium-enhanced cardiovascular magnetic resonance imaging. *JACC*, 47:370-378, 2006.
[3] Krahn P.R.P., *et al.*, Cardiovascular magnetic resonance guided ablation and intra-procedural visualization of evolving radiofrequency lesions in the left ventricle. *JCMR*, 20:20, 2018.
[4] Kawamura I., *et al.*, Electrophysiology, pathology, and imaging of pulsed field ablation of scarred and healthy ventricles in swine. *Circ A E*, 16:e011369, 2023.
[5] Escartin T., *et al.* Comparing RFA and PFA scar homogenization in a chronic swine model of infarction using 3D LGE MRI. *Heart Rhythm*, 20:S458-S459, 2023.
[6] Nakatani Y., *et al.* Pulsed field ablation prevents chronic atrial fibrotic changes and restrictive mechanics after catheter ablation for atrial fibrillation. *Europace*, 23:1767-1776, 2021.
[7] Regany-Closa M., *et al.* Head-to-head comparison of pulsed-field ablation, high-power short-duration ablation, cryoballoon and conventional radiofrequency ablation by MRI-based ablation lesion assessment. *J Interv Card Electrophysiol*, 2025.
[8] Hermans B.J.M., *et al.* Visualization of monopolar biphasic focal pulsed field ablation lesions 3 months after pulmonary vein isolation on high-resolution 3-dimensional dark-blood late gadolinium enhancement cardiac magnetic resonance images. *Heart Rhythm*, 23:243-248, 2026.
[9] Jerltorp K., *et al.* Multimodal MRI-based assessment of atrial acute and chronic radiofrequency and pulsed field ablation lesion characteristics in a porcine model. *Europace*, 28(Suppl 1):i1087, 2026.

Collateral effects of electroporation: heating, electrical stimulation, and electrochemical reactions

Antoni Ivorra; *Department of Engineering, Universitat Pompeu Fabra, Carrer Roc Boronat 138, 08018 Barcelona, SPAIN*

INTRODUCTION

Applying electrical energy to living tissues for inducing electroporation can cause diverse phenomena in addition to electroporation. Three well-identified collateral phenomena, which in most cases are undesired, are heating, electrical stimulation, and electrochemical reactions.

HEATING

Except for superconductors, all electrical conductors dissipate electrical energy in the form of heat when current flows through them. This phenomenon is known as Joule heating or resistive or Ohmic heating and obeys:

$$P = I^2 R$$

where P is the power of heating, I is the current flowing through the conductor and R is its resistance. This equation, known as Joule's law, can also be expressed for infinitesimal volumes at each point of space:

$$p = \frac{\left|\vec{J}\right|^2}{\sigma} = \left|\vec{E}\right|^2 \sigma$$

where σ is the electrical conductivity and $\vec{J}$ and $\vec{E}$ are the current density and electric field respectively. In electroporation scenarios, with field magnitudes in the order of hundreds of V/cm and conductivities in the order of S/m, Joule heating would cause harmful temperatures if very short exposures, much shorter than a second, were not used. The dependence of heating on the square of the electric field is relevant because it implies that heating is particularly high where the electric field is larger, typically at the periphery of the electrodes due to the edge effect. This is further exacerbated by the increase of σ with the temperature.

The temperature increase due to the Joule effect can be accurately predicted with numerical models, even for complex tissues. However, thermal damage models used to predict the physiological impact of the intense temperature peaks caused during electroporation are intended for longer exposures and, although are used by the electroporation community, their accuracy is still unknown.

ELECTRICAL STIMULATION

The nervous system transmits signals in the form of action potentials. Action potentials are sudden transitions in transmembrane resting voltage that propagate along the cell. Electrical stimulation consists in nonphysiologically triggering action potentials by delivering electric fields.

In clinical applications of electroporation, electrical stimulation is not desired because, by exciting efferent nerves, it causes muscle contractions and, by exiting afferent nerves, it causes pain [1].

Both electroporation and electrical stimulation occur when the transmembrane voltage is artificially increased above a threshold due to the presence of the electric field. This implies that unsought stimulation occurs very frequently when electroporation is intended. Advantageously, high-frequency biphasic fields can cause electroporation whilst minimizing electrical stimulation [2].

ELECTROCHEMICAL REACTIONS

Electrical conduction in metallic electric circuits is provided by the flow of electrons whereas in living tissues (and in suspensions) the moving charge carriers are ions. Conduction across the interface between the electronic conductor and the ionic conductor, that is, across the electrode, can be capacitive or electrochemical. Capacitive conduction is only substantial for very brief or ac currents of small magnitude. In most electroporation scenarios, conduction across the electrode is mediated by electrochemical reactions. In electrochemical reactions, the chemical species in the living tissue and the electrode exchange electrons thus altering their chemistry.

Electrochemical reactions are generally deleterious for electroporation applications because they modify pH and cause the release of gases and metallic ions. (However, it is worth noting that it has been proposed their synergy with electroporation to achieve large ablation volumes [3]).

Electrochemical reactions are a surface phenomenon (occur at the electrode) and, because of that, are of particular concern when the electrode area is large compared to the treated volume, as is typically the case in microfluidic setups.

Electrochemical reactions are difficult to model, particularly at the anode (positive electrode) because multiple reactions can occur concurrently.

Interestingly, high-frequency biphasic currents minimize electrochemical reactions. This effect, combined with lower stimulation, explains the emergence of high-frequency biphasic fields for electroporation-based ablation.

REFERENCES

[1] Cvetkoska A., et al. Muscle contractions and pain sensation accompanying high-frequency electroporation pulses. Sci Rep,12:8019, 2022.

[2] Mercadal B., et al. Avoiding nerve stimulation in irreversible electroporation: a numerical modeling study. Phys Med Biol, 62:8060-8079, 2017.

[3] Klein N., et al. Single exponential decay waveform; a synergistic combination of electroporation and electrolysis (E2) for tissue ablation. PeerJ, 5:e3190, 2017.

Fundamental principles of designing safe, effective, and usable systems for cardiac ablation via pulsed electric fields

Brendan Koop; *Electrophysiology Research and Development, Boston Scientific Corporation, 4100 Hamline Ave N, Arden Hills, MN, USA*

INTRODUCTION

This lecture will review fundamental principles for optimizing cardiac pulsed field ablation (PFA) system design. Though modern PFA has revolutionized treatment for arrythmias like atrial fibrillation (AF), getting to this point took decades. The first approaches to endocardial ablation for the treatment of cardiac arrhythmias arose in the 1980's as a less invasive alternative to open heart cardiac surgical methods [1]. These approaches utilized diagnostic electrophysiology (EP) catheters and high voltage direct current pulses generated from external cardioverter defibrillators as a kind of first form of PFA. Adverse effects from some of these ablations pushed the field of EP to thermal ablation modalities [2]. However, the desire to also lessen thermal adverse effects, the need for workflow improvements to treat more patients, and improvement in generator and catheter technology have brought PFA back to being the standard of care for AF ablation therapy [3,4].

OPTIMIZATION OF PFA

The goal of a cardiac PFA system is to provide safe, effective, and usable therapy for the treatment of cardiac arrhythmias (Figure 1). As this lecture reviews, achieving this goal is a complex exercise in system design, requiring optimization of catheter, waveform, and dosing. This optimization is often iterative, as myriad design factors are balanced to achieve the goal while making use of computational modeling, bench testing, preclinical animal studies, and human clinical studies to evaluate system performance [5].

FUTURE DIRECTIONS

Work remains to further optimize cardiac PFA systems and workflows, as the lecture describes. Like all ablation modalities, PFA has its own potential adverse effects that can be further minimized. Efficacy of atrial PFA lesion sets has not reached 100%, even for pulmonary vein isolation for the treatment of AF, and even less so for other atrial anatomical targets involving thicker tissue. Additionally, ablation tools and techniques for the treatment of ventricular tachycardia have historically been underdeveloped due to lower procedure volume relative to atrial arrhythmias. Cardiac PFA systems can be further developed and optimized to address these challenges by adhering to fundamental principles discussed here.

REFERENCES

[1] Gallagher J. J., *et al*. Catheter Technique for Closed-Chest Ablation of the Atrioventricular Conduction System. *NEJM*, 306:194-200, 1982.
[2] Huang S. K., *et al*. Closed Chest Catheter Desiccation of the Atrioventricular Junction Using Radiofrequency Energy–A New Method of Catheter Ablation. *JACC*, 9:349-358, 1987.
[3] Reddy V. Y., *et al*. Ablation of Atrial Fibrillation with Pulsed Electric Fields: An Ultra-Rapid, Tissue-Selective Modality for Cardiac Ablation. *JACC:CE*, 4:987-985, 2018.
[4] Chun K. J., *et al*. State-of-the-art Pulsed Field Ablation for Cardiac Arrhythmias: Ongoing Evolution and Future Perspective. *Europace*, 26, 2024.
[5] Koop B. E. Fundamentals of System Design for Cardiac Pulsed Field Ablation: Optimization of Safety, Efficacy, and Usability. *PACE*, 49:5-14, 2026.

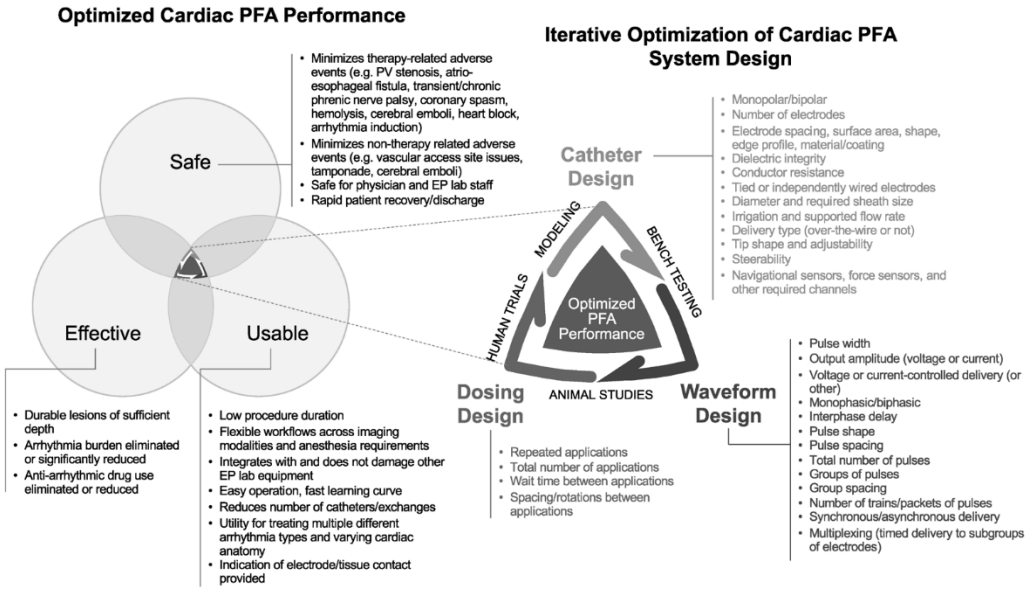


Figure 1: Graphical depiction of optimized cardiac PFA performance and the iterative optimization of cardiac PFA system design to achieve a safe, effective, and usable system.[5]

Irreversible electroporation as an ablation technique

Rafael Davalos; *Department of Biomedical Engineering, Georgia Tech, Atlanta, USA*

INTRODUCTION

Irreversible Electroporation (IRE) is a minimally invasive tissue ablation technique that involves applying low-energy pulses to create nanoscale defects in the lipid bilayer, inducing cell death. [1]. High frequency irreversible electroporation (H-FIRE) [2], otherwise known as biphasic Pulsed Field Ablation (PFA), is a next-generation form of IRE and is being used for the treatment of cardiac arrhythmias, cancer, and other malignancies. This new therapy mitigates the need for intraoperative paralytics to prevent involuntary pulse-related muscle contractions. IRE and H-FIRE are unique among ablation techniques, as they only affect the cell membrane while tissue molecules such as collagen structures and proteins remain intact, thereby making treatment near previously inoperable critical structures possible. Further, they facilitate a robust immune response by releasing damage-associated molecular pathways (DAMPs) and disease-specific antigens in their native state [3].

By modifying the pulse parameters and field strength, the ablation can be tuned to specific modes of cell death [5] to produce non-inflammatory (e.g., apoptosis) or pro-inflammatory (e.g., necrosis, pyroptosis, and necroptosis) responses [3,4]. We will discuss these mechanisms and their effect on the innate and adaptive immunological response.

We will also discuss numerical modeling techniques to accurately predict the field distributions and corresponding ablation volumes within the tissue as a function of these waveforms.

As electroporation occurs, the permeability of ions across the cellular membrane increases, causing the bulk conductivity to rise. This is captured by treating the conductivity of the tissue as a dynamic variable which is a function of the local electric field to which the specific tissue is exposed to for a given pulse parameter. We often describe this as a conductivity curve, using the logistic sigmoid curve. The initial conductivity of the tissue, σ_0, and the electroporation midpoint, E_{del}, are primarily affected by the pulse width and pulse number, while the final conductivity, σ_f, often held constant between different pulse widths and numbers [6,7,8].

Tertiary but critically important, effects such as electrolysis can also be captured by modeling the conductivity curve as a double sigmoid [9]. This work is in the early stages but may enhance our abilities to accurately predict treatment. Similar to the initial conductivity curve, this new formulation follows a second logistic sigmoid curve, and we consider that the electrolysis if formed in regions where the electric field is above the electrolysis electric field threshold, E_{ep}, and that regions has the final conductivity, σ_{eb}.

The conductivity curve is given by the following:

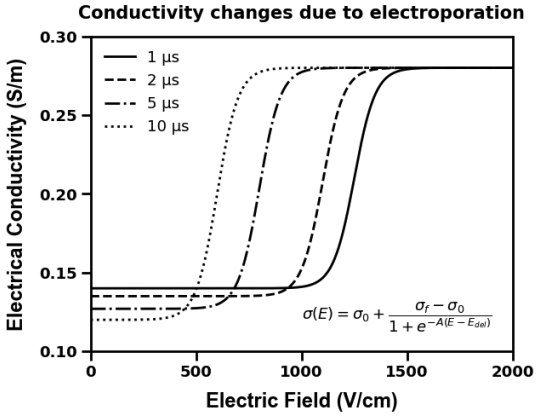
$$\sigma(|E|) = \sigma_0 + \frac{\sigma_f - \sigma_0}{1 + \exp(-A(|E| - E_{del}))} + \frac{\sigma_{eb} - \sigma_f}{1 + \exp\left(-A(|E| - E_{ep})\right)}$$

Finally, this lecture will cover recent advances in pulsed electric field therapies to target other aspects of the tumor microenvironment and potential clinical applications.

In addition to modeling the field distribution, we will discuss how to accurately model the temperature distribution as a function of various pulse parameters, which is crucial for mitigating thermal damage in many of these applications.

$$\rho c_p \frac{\partial T}{\partial t} = \nabla \cdot (k \nabla T) + \omega_b \rho_b c_{p,b} (T_a - T) + \dot{q}_m + \dot{q}_j$$

$$\dot{q}_j = \sigma |\nabla \Phi|^2 \tau$$



REFERENCES

[1] Davalos R.V., *et al*. Tissue ablation with IRE. *Ann Biomed Eng*, 33:223-231, 2005.

[2] Arena C.B., *et al*. Theoretical considerations of tissue electroporation with high-frequency bipolar pulses. *IEEE Trans Biomed Eng*, 58, 2011.

[3] Ringel-Scaia V.M., *et al*. High-frequency IRE is an effective tumor ablation strategy that induces immunologic cell death and promotes systemic anti-tumor immunity. *EBioMedicine*, 44, 2019.

[4] Mercadal B., *et al*. Dynamics of cell death after conventional IRE and HFIRE treatments. *Ann Biomed Eng*, 48, 2020.

[5] Polajzer T., *et al*. Immunogenic cell death in electroporation-based therapies depend on pulse waveform characteristics. *Vaccines*, 11, 2023.

[6] Jacobs E.J., *et al*. Comprehensive characterization of waveform dependent cardiac tissue electroporation for PFA. *Biosens Bioelectron,* 289: 117890, 2025.

[7] Jacobs E.J., *et al*. Effects of interphase and interpulse delays on tissue impedance and PFA. *Ann Biomed Eng*, 53:1962-1974, 2025.

[8] Jacobs E.J., *et al*. Characterizing reversible, irreversible, and calcium electroporation to generate a burst-dependent dynamic conductivity curve. *Bioelectrochemistry*, 144:108580, 2024.

[9] Salameh Z., *et al*. Acoustic effects during PFA: measurement and control of bubble and void formation, *J Colloid Interface Sci*, 727:141584, 2027.

Atrial fibrillation from genes to therapeutics

Mina K. Chung, MD; *Cardiac Electrophysiology and Pacing, Dep.of Cardiovascular Medicine, Heart, Vascular & Thoracic Institute, Dep. of Heart, Blood & Kidney Research, Cleveland Clinic Research, Cleveland Clinic, Cleveland Clinic Lerner College of Medicine of Case Western Reserve University, Cleveland, Ohio, USA*

INTRODUCTION

Atrial fibrillation (AF) is the most common sustained arrhythmia, affecting over 50 million people worldwide. AF is associated with heterogeneous cardiovascular stressors, including aging and obesity, as well as risk for stroke, heart failure and atrial cardiomyopathy. With studies reporting significant heritability and genome wide association studies (GWAS) finding multiple genetic loci associated with risk for AF, potential opportunity exists to identify upstream targets and therapies.

AF GWAS

A strong locus at chromosome 4q25 was found by initial GWAS. The gene nearest this locus is *PITX2.* The cardiac isoform PITX2c is associated with formation of the pulmonary veins, the target of today's pulsed field ablation approaches to AF. Over the next decade, larger GWAS have reported over 300 loci associated with risk for AF. The top loci remain at chr. 4q25.

FROM GWAS TO AF MECHANISMS

PITX2 is a transcription factor expressed in the left atrium during cardiac development. However, AF does not usually present until decades later. Using whole genome transcriptomics in human left atrial tissues, we have taken approaches to identify the causative variants and genes at GWAS-identified AF risk loci and to identify pathways associated with AF using functional genomics, coexpression and pathway analyses.

DUAL RISK MODEL FOR AF

Transcriptomic analyses in human left atrial tissues with and without AF showed reduced transcriptional responses to cell stress.[1] Metabolic, oxidative and other stress pathways were confirmed in gene coexpression analyses of the top AF GWAS implicated genes.[2] This led to our dual risk model for AF, where in genetically susceptible individuals, who are born with genetic susceptibility to pulmonary vein triggers from genes active in development, that inadequate transcriptional responses to stress predispose to AF in later life. Such stressors include aging, obesity, metabolic stress, mitochondrial dysfunction, oxidative stress, and abnormal proteostasis.[2] These pathways represent potential targets for upstream therapies.

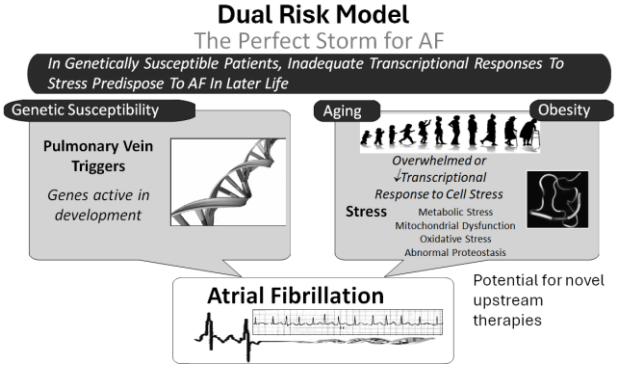


Figure 1. Dual Risk Model for AF

NETWORK SYSTEMS BIOLOGY APPROACHES TO DRUG REPURPOSING

Network systems biology approaches to drug repurposing and discovery incorporates layers of data related to biological systems and environmental factors to identify disease networks and potential drug targets. Genetically supported targets may increase clinical development success rates.

Our first generation disease module incorporated human atrial RNASeq transcriptomics and identified several potential candidate drugs, one of which is metformin, which targets AMP kinase, a master regulator of metabolic stress.[3]

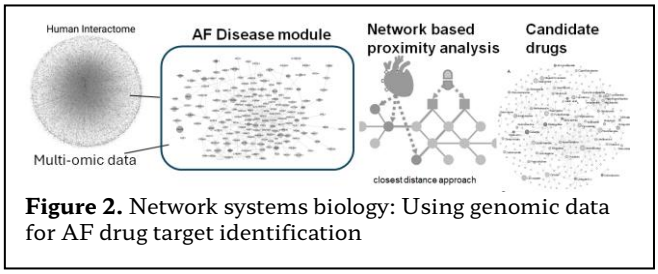


Figure 2. Network systems biology: Using genomic data for AF drug target identification

BACK TO THE BEDSIDE TO TEST A CANDIDATE DRUG

We tested metformin in inducible pluripotent stem cell (iPSC)-derived cardiomyocytes and are currently testing it in a clinical trial (TRIM-AF), but the drug's tolerability is limiting.

CURRENT AND FUTURE

Newer metabolic agents may be more effective or tolerable, and we are refining the network approaches with additional 'omics inputs and cardiomyocyte drug targeting, as well as pursuing candidate gene approaches for structural based drug discovery and design.

REFERENCES

[1] Deshmukh A., *et al.* Left atrial transcriptional changes associated with atrial fibrillation susceptibility and persistence. *Circulation Arrhythm Electrophysiol*, 8:32-41, 2015.

[2] Wass S.Y., *et al.* Novel functional atrial fibrillation risk genes and pathways identified from coexpression analyses in human left atria. *Heart Rhythm*, 20:1219-1266, 2023.

[3] Lal J.C., *et al.* Transcriptomics-based network medicine approach identifies metformin as a repurposable drug for atrial fibrillation. *Cell Rep Med*, 3:100749, 2022.

Vascular effects in electroporation-based treatments

Bostjan Markelc[1, 2]; [1]*Department of Experimental Oncology, Institute of Oncology Ljubljana, SLOVENIA;* [2]*Department of Biology, Biotechnical Faculty, University of Ljubljana, SLOVENIA*

INTRODUCTION

Electroporation/electropermeabilization (EP), i.e. the application of electric pulses to cells or tissue, leads under suitable conditions to a reversible permeabilization of the cell membranes and thus facilitates the entry of exogenous molecules into the cells. Reversible EP of tissue is feasible, efficient and tolerable in humans. The most advanced routine clinical application is electrochemotherapy (ECT), in which cytotoxic drugs are delivered to cells to treat tumors. More recently, this approach has also been used in the treatment of vascular malformations, where it has been termed bleomycin electrosclerotherapy (BEST). If excess electric pulses are applied, this leads to irreversible electroporation (IRE). The use of IRE to treat various types of cancer is intensively researched and several clinical trials are ongoing. In addition, IRE has recently been successfully adapted for the treatment of cardiac arrhythmias, where it is referred to as pulsed field ablation (PFA). Since the early experiments with EP and ECT in mouse tumors, it became clear that the EP-based treatments have an effect on the normal and tumor vasculature in addition to the direct cytotoxic effect of the therapy on the tumor cells. This is now directly exploited in BEST and is also recognized as adverse event in the treatment of cardiac arrhythmias.

RESPONSE OF ENDOTHELIAL CELLS TO ELECTROPORATION

Endothelial cells, which form the inner lining of blood vessels, exhibit varying sensitivity to EP depending on electric field intensity, pulse duration, and tissue type. In vitro studies on human endothelial cells have shown that reversible EP induces cytoskeletal changes, most notably disruption of actin and tubulin filaments, followed by disruption of cell-to-cell junctions, which control vascular permeability [1]. Moreover, in vitro studies demonstrated that EP increases the permeability of endothelial monolayers in a dose-dependent manner.

DIFFERENTIAL EFFECTS OF EP AND ECT ON NORMAL AND TUMOR BLOOD VESSELS

The application of EP pulses to normal blood vessels increases the permeability of the affected blood vessels, causes transient vascular lock, i.e. a decrease in perfusion, and modulates the diameter of the affected blood vessels. Similarly, the application of EP or ECT to tumors increases the permeability of the affected blood vessels and causes vascular lock [2]. In normal blood vessels, these effects are short-lived, whereas in tumor vessels they are long-lasting and persist more than 72 hours after ECT.

In tumors, EP leads to an immediate abrogation of blood flow, i.e. a vascular lock that lasts for more than 60 min. Interestingly, the tumor-supplying arterioles react to EP in the same way as normal vessels, namely with rapid vasoconstriction and increased permeability [3]. This suggests that this is the main cause of the immediate vascular lock observed after EP. EP also leads to increased permeability of tumor blood vessels to macromolecules and a partial, long-lasting decrease in perfusion. Thus, EP has a differential effect on normal and tumor blood vessels. Moreover, ECT has a direct cytotoxic effect on tumor endothelial cells, i.e. it has a vascular disrupting effect, which is now also exploited in BEST.

EFFECTS OF IRE ON BLOOD VESSELS

The effects of IRE on blood vessels were first confirmed with magnetic resonance imaging (MRI) of perfusion in the rat brain after EP, showing that IRE increases the permeability of blood vessels to macromolecules [4]. Importantly, further studies conducted on various normal blood vessels showed that while IRE can destroy the endothelial cells, the large blood vessels retain their functionality and are repopulated with endothelial cells after therapy.

CONCLUSIONS

In summary, EP-based treatments have effects on the endothelial cells and thus on the normal and tumor vasculature. This can be exploited to destroy endothelial cells, as is the case with ECT and BEST, or one can rely on their function-preserving property when it comes to normal blood vessels, as is the case with IRE and PFA.

REFERENCES

[1] Kanthou C., *et al*. The endothelial cytoskeleton as a target of electroporation-based therapies. *Mol Cancer Ther*, 5:3145-52, 2006.

[2] Jarm T., *et al*. Antivascular effects of electrochemotherapy: implications in treatment of bleeding metastases. *Expert Rev Anticancer Ther*, 10:729-46, 2010.

[3] Markelc B., *et al*. Differential mechanisms associated with vascular disrupting action of electrochemotherapy: intravital microscopy on the level of single normal and tumor blood vessels, *PLoS One*, 8: e59557, 2013.

[4] Hjouj M., *et al*. MRI study on reversible and irreversible electroporation induced blood brain barrier disruption. *PLoS One*, 7: e4281, 2012.

RNA therapies for cardiac repair and regeneration

Mauro Giacca[1,2]; *[1]School of Cardiovascular and Metabolic Medicine & Sciences; [2]MRC/BHF Centre of Research Excellence for Advanced Cardiac Therapies (REACT), The James Black Centre, 125 Coldharbour Lane, London SE5 9NU, UNITED KINGDOM*

Cardiac disorders are common, lethal and expensive. Heart failure, which is a consequence of most cardiac conditions, now affects over 1-3% of the global adult population, has a 5-year mortality of 40-50% and absorbs 2-3% of national health expenditures in high-income countries. Cardiomyocyte death is not offset by new cell generation after birth, as the regenerative capacity of the adult human myocardium is less than 1% per year over a lifetime. To date, no drug exists for myocardial survival or regeneration, nor any gene editing therapy for the correction of genetic defects. More in general, no biological therapy has ever been developed for any primary cardiac condition.

A main goal of my laboratory is to develop RNA therapeutics to treat cardiac disease, with the objectives of preventing cardiomyocyte loss after damage, stimulating cardiac regeneration and achieving precise gene editing for the correction of hereditary cardiac mutations. We identify effective RNAs through unbiased, functional, high throughput screenings in vitro and in animal models.

To prevent myocardial damage, we screened a library of 1200 proteins from the secretome and identified three effective anti-apoptotic and pro-autophagic factors. The delivery of the mRNA of one of these proteins to the liver, followed by its secretion into the bloodstream, prevents cardiac damage after myocardial infarction. For cardiac regeneration, we are progressing four microRNA that stimulate cardiomyocyte proliferation towards clinical translation in patients with myocardial infarction. For the correction of the mutations underlying inherited cardiomyopathies, we identified two families of microRNAs that stimulate precise gene editing by reawakening expression of the homologous recombination machinery in post-mitotic, adult hearts.

We achieve expression of our mRNAs and microRNAs either using AAV vectors or by embedding the RNAs in lipid nanoparticles (LNPs) generated with the SNALP technology, which are amenable to clinical translation in patients.

Irreversible electroporation for the use of cardiac ablation

Atul Verma, MD; *Faculty of Medicine, McGill University, Montreal, Quebec, CANADA*

INTRODUCTION

Historically, cardiac ablation for the treatment of cardiac arrhythmias was performed using thermal energy sources, namely radiofrequency and cryothermy. While these techniques were employed for decades, the use of irreversible electroporation has now been implemented in the treatment of cardiac arrhythmia, particularly for atrial fibrillation (AF). For arrhythmia treatment, we call this energy source "pulsed field ablation" (PFA).

LIMITATIONS OF THERMAL ENERGY

Thermal energy produces effective lesions in the heart for most cardiac arrhythmias. The traditional tissue depth of these lesions ranges from 4-7 mm.

For AF, the strategy of cardiac ablation is based on electrical isolation of the pulmonary veins from the rest of the left atrium. The pulmonary veins are the main source of triggers for AF. Thermal energy tissue depths were adequate for ablation, but there was always a small risk of collateral damage to tissues adjacent to the left atrium. In particular, the phrenic nerve is located near the right superior vein and damage to this nerve occurred in 2-5% of cases with cryothermy. The esophagus is located behind the left atrium and it could be damaged in 0.5% of cases, and even lead to fatal atrio-esophageal fistula formation in 1/2000 cases.

For ventricular arrhythmias, the depth of 4-7 mm was not enough for walls that could be in excess of 10 mm thick. Furthermore, radiofrequency had limited ability to penetrate scars in the ventricle which are often the cause of re-entrant arrhythmias.

BENEFITS OF PULSED FIELD ABLATION

PFA has been rapidly adopted for ablation of AF because of its improved safety profile compared to thermal energy. While subclinical damage is still possible to both the esophagus and phrenic nerve from PFA application, these tissues will heal over hours to days because PFA preserves the extracellular matrix. Thermal energy destroys the matrix, not allowing progenitor cells to repopulate and heal the tissue. PFA also does not cause any risk of stenosis of the pulmonary veins when applied inside the vein. To date, there have been no reported cases of permanent phrenic palsy, esophageal fistula, or pulmonary vein stenosis secondary to PFA.

Another major advantage of PFA is its speed of use. Since pulses are delivered in an H-FIRE style with microsecond durations, ablations can be completed in a fraction of the time compared to older thermal energies. AF ablations that once took 60 to 90 minutes to complete can now be completed in 30-60 minutes.

It was hoped that PFA may offer better efficacy compared to thermal ablation, but several clinical trials comparing the 2 energy sources failed to show a difference in efficacy.

NEW PROBLEMS WITH PFA

Although many trials and registries have confirmed the safety of PFA, some novel complications have occurred with this technology. First, it has been noted that application of PFA in proximity to the coronary arteries can cause acute spasm which can lead to life-threatening cardiac ischemia. This occurs particularly on the cavotricuspid isthmus, the mitral isthmus, and in the epicardium. Nitroglycerin intravenously may prophylax against this, but the dosing regimen required is still a matter of ongoing investigation. Delayed spasm several hours or days after the ablation can also occur but seems to be related to a high number of applications and not proximity to the coronaries. This could be due to patient factors and nitric oxide depletion due to hemolysis.

Hemolysis also occurs to different extents with PFA technologies. Some cause clinically significant hemolysis which can cause acute kidney injury which can be mitigated by fluid loading. However, nitric oxide depletion will still occur.

REFERENCES

[1] Verma A., *et al*. Primer on pulsed electrical field ablation: understanding the benefits and limitations. *Circ Arrhythm Electrophysiol,* 14: e10086, 2021.

[2] Anic A., *et al*. Pulsed field ablation: from concepts to technology. *EP Europace,* 28: ii18-ii31, 2026.

It begins at the end - how clinical goals and constraints affect electroporation device development

Michael B. Sano; *Department of Molecular Biomedical Sciences, North Carolina State University, Raleigh, NC, USA*

INTRODUCTION

Medical devices have long development timelines and even longer commercial lifetimes. A new system may require years of engineering, testing, and regulatory review before reaching the clinic, yet remain in use for decades with few substantive changes to its underlying capabilities. During that time, advances in biophysics, electronics, and treatment planning may enable superior solutions. However, the cost and regulatory complexity of redesign often favor incremental modifications over significant technological advances.

These extended product lifetimes, coupled with the substantial cost of commercialization, make early design decisions especially consequential. This lecture will examine the medical device development and commercialization process, emphasizing the importance of beginning with an unmet clinical need and working backward from the regulatory pathway to establish appropriate engineering specifications.

ECONOMICS AND REGULATORY CONSTRAINTS

Developing a new pulse generator and applicator can cost well over US$10 million, excluding clinical trials, regulatory submissions, and good laboratory practice (GLP) studies. Early design decisions establish constraints that influence risk management, manufacturing, verification and validation, and ultimately regulatory approval. As a device approaches regulatory submission or market authorization, substantive design changes may necessitate costly redesign, repeated testing, and additional regulatory review. Consequently, decisions made for short-term engineering convenience can accumulate technical and regulatory debt, making late-stage corrections disproportionately expensive, often at a critical point when securing additional capital is particularly challenging.

DESIGNING BACKWARD FROM THE REGULATORY ENDPOINT

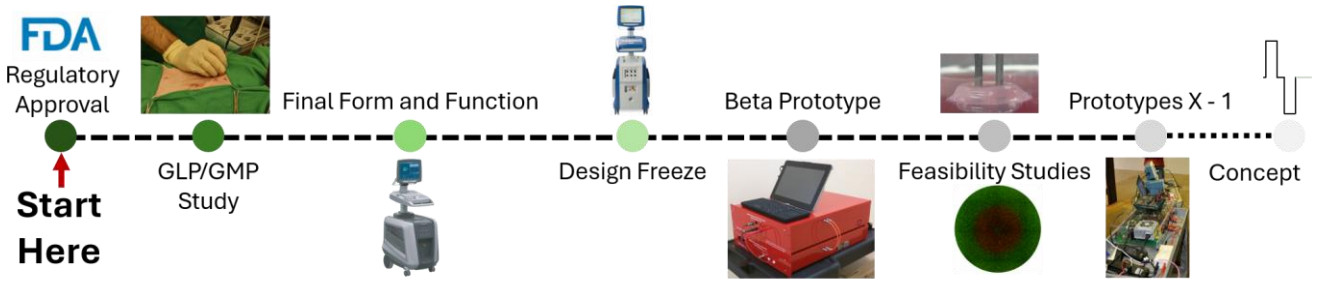
Effective device development should begin with a clearly defined unmet clinical need, intended therapeutic outcome, procedural workflow, and, critically, a viable regulatory pathway. Establishing the regulatory strategy early enables the development of appropriate risk management, verification, and validation plans before the device architecture becomes fixed. These requirements may impose unexpected constraints on device capabilities or necessitate additional design complexity that would be substantially more difficult to accommodate later in development.

For electroporation technologies, it is particularly important that engineering specifications be grounded in well-established biophysical principles and robust preliminary data that can be extrapolated to clinically relevant conditions. This lecture will explore how regulatory and safety requirements, including electrical isolation and patient monitoring, can constrain device capabilities and introduce challenging trade-offs between safety, technical performance, and clinical effectiveness.

CONCLUSIONS

In a highly regulated environment, early engineering decisions can become long-term clinical limitations. Meaningful translation requires working backward from the clinical objective and regulatory strategy to identify biophysical and engineering solutions that are not only technically feasible, but capable of delivering safe, reproducible, and durable clinical outcomes.

Figure 1: Product Trajectory from Concept to Regulatory Approval.





SHORT PRESENTATIONS BY STUDENTS AND PARTICIPANTS

Live cell imaging and microdosimetry assessment of electroporation: an integrated in vitro and in silico approach

Gianmarco Ronza[1,2], Anna Sannino[2], Fabiana Di Costanzo[2,3], Mariateresa Allocca[2], Olga Zeni[2], Maria Rosaria Scarfì[2], Luigi Zeni[1], Stefania Romeo[2]. *[1]Dept. of Engineering, University of Campania "Luigi Vanvitelli", Aversa, ITALY; [2]Institute for Electromagnetic Sensing of the Environment, Italian National Research Council, Naples, ITALY; [3]Dept. of Precision Medicine, University of Campania "Luigi Vanvitelli", Naples, ITALY*

INTRODUCTION

Despite their widespread use in biomedicine and biotechnology, electroporation (EP)-based applications are often limited by an incomplete understanding of the physical and biological mechanisms governing the phenomenon [1]. In this study, by taking advantage of live cell imaging, a methodology for microdosimetric assessment of EP has been developed to improve biophysical understanding of the phenomenon. To this aim, *in vitro* and *in silico* approaches were integrated.

METHODS

A375 human melanoma cells grown onto a glass coverslip were placed in contact with two parallel plane electrodes made by aluminium tape on a microscope slide. The electrodes' gap was filled with Phosphate Buffered Saline (PBS) and Propidium Iodide (PI) to monitor EP. The cells were housed in a custom support fitting the stage of a Leica TCS SP5X confocal microscope for real-time observations. Time-lapse acquisition recorded the fluorescence intensity pre-, during, and post-delivery of 16 pulses (100 µs duration, 1 Hz, 600-1200 V/cm), provided by an ELECTROcell-B15 high voltage pulse generator (Leroy Biotech, France). Baseline PI fluorescence intensity (sham control) was recorded during the first 20 seconds and used as an internal reference for Regions of Interest (ROIs) signal normalization.

A multi-physics finite element method study was developed in COMSOL Multiphysics© (ver. 6.4) emulating the experimental set-up. A cluster of 9 cells positioned within the PBS domain was implemented to represent a simplified version of the experimental exposure chamber. Realistic morphologies, obtained through a customized semi-automatic procedure, were considered. Periodic boundary conditions were applied along the YZ-plane to emulate the surrounding experimental domain while maintaining computational efficiency. Mesh independence was validated through Richardson extrapolation and Grid Convergence Index analysis (GCI < 2%), justifying the adoption of the finest mesh for studies [2]. The microdosimetry analysis at 1200 V/cm exposure condition is reported here to show the effective local distribution of the electric field.

RESULTS

Fig.1 shows that EP yield increases upon increasing the electric field. However, within each pulse condition, a great variability was recorded in the cellular response which prevents the expected dose-response behaviour. *In silico* analysis provided an aid in the interpretation of *in vitro* results. As matter of fact, an inhomogeneous electric field distribution was revealed with localized peaks among cells in closer proximity (inset of Fig.2). This was due to the inclusion of realistic features in the numerical model such as cell density, spatial arrangement, irregular morphologies and intercellular proximity.

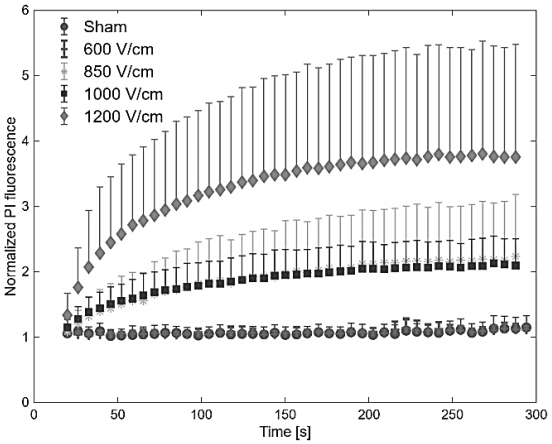


Figure 1: Time-course of normalized PI fluorescence intensity in A375 cells exposed to 16 pulses (100 µs, 1 Hz) at 600–1200 V/cm. Each point represents the mean of at least 3 independent experiments (at least 30 ROIs for each experiment). To ensure a clean data visualization, only positive standard deviation bars are shown.

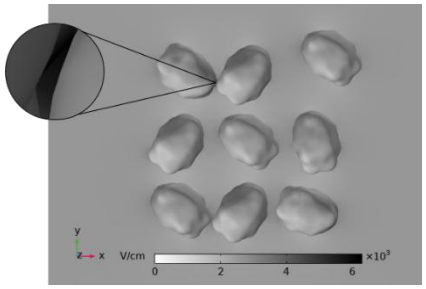


Figure 2: Electric field distribution in a cluster of 9 cells with realistic morphologies and arrangement exposed to 1200 V/cm. The inset shows a localized peak of the electric field between adjacent cells.

CONCLUSIONS

We demonstrated here that the proposed approach, integrating live cell imaging and numerical microdosimetry analysis, effectively supports mechanistic understanding of EP.

REFERENCES

[1] Aycock K. N., *et al.* doi: 10.1089/bioe.2019.0029, 2019.
[2] Oberkampf W. L., *et al.* doi: 10.1017/CBO9780511760396, 2010.

OpenDEP: a modular open-source platform for population or single-cell dielectrophoretic characterization of cells

Ioan Tivig, Florela Gherghinoiu, Mihaela G. Moisescu, Tudor Savopol; *Biophysics and Cellular Biotechnology Department, Faculty of Medicine, "Carol Davila" University of Medicine and Pharmacy, Bucharest, ROMANIA*

INTRODUCTION

Dielectrophoresis (DEP) moves polarizable particles in a non-uniform alternating electric field, with a magnitude and direction that depend on the field frequency and on the cell's electrical properties. Fitting the resulting DEP spectrum with a shell model gives the conductivity and permittivity of the membrane and cytoplasm, making DEP a label-free, non-destructive way to characterize cells. Few instruments record full DEP spectra: the most popular commercial DEP characterization systems use disposable chips and a fixed number of frequencies, while laboratory set-ups usually give only the crossover frequency.

We previously introduced OpenDEP, an open-source platform made of a lab-on-a-chip and analysis software, validated against the commercial 3DEP reader [1]. It has since been used to characterize oxidized retinal pigment epithelial cells as a model of age-related macular degeneration [2] and extended to iterative single-cell DEP and optical characterization [3]. Its first version, however, relied on a conventional microscope and manual operation. Here we present how OpenDEP is being redesigned as a modular, stand-alone instrument with an integrated software suite.

PLATFORM CONCEPT AND HARDWARE

The concept follows three principles: I. the device is self-contained and needs no external microscope; II. it is modular: each function is an independent, replaceable module; III. it is open: all hardware documentation and software are publicly released.

The instrument is built around four hardware modules: (1) The *OpenDEP lab-on-a-chip*, slightly changed from the validated design [1]: two indium tin oxide-coated glass slides with laser-engraved electrodes, held in a 3D-printed body that forms a closed, openable and washable chamber that keeps cells in focus and allows sterile work. (2) A *function generator* that applies a sinusoidal signal of up to 20 Vpp between 1 kHz and 50 MHz. (3) A *precision pump* (0.1 µL/s to 10 mL/s) that loads the suspension, homogenizes it between frequency steps and cleans the chamber afterwards. (4) An *integrated imaging module* with collimated illumination, a 4× objective and a camera, which records how the cells are distributed along the electrodes. Commercial modules (generator, pump, control computer) are combined with custom 3D-printed illumination, optics and enclosures. A microcontroller drives the generator, pump and illumination; the camera connects directly to the control computer. Any module can be swapped for an equivalent device.

SOFTWARE: CONTROL, COMPUTE, VIEW

Three open-source applications cover the workflow:

OpenDEP Control drives the instrument. It sets frequency and voltage, controls flow and illumination, and runs automated protocols: frequency sweeps, homogenization between steps, and image capture at each frequency.

OpenDEP Compute turns the acquired images into DEP spectra from the images with cell population distribution. It fits single-shell or homogeneous-sphere models by non-linear least squares to extract membrane permittivity and conductivity and cytoplasmic conductivity. Compute is hardware-independent: it was used to fit 3DEP-recorded spectra of mesenchymal stem cells during early differentiation [4].

OpenDEP View is used to explore the results. It compares spectra across samples, simulates spectra from given dielectric parameters, and exports well formatted figures.

RESULTS AND DISCUSSION

The stand-alone instrument is in the design and manufacture phase. The lab-on-a-chip is already built, and the analysis software is already validated. OpenDEP spectra and fitted parameters for DC3F and NIH 3T3 cells agreed with the 3DEP reader within standard deviation, with lower variability [1]. Integrated imaging and automated sweeps and sample handling remove the two main drawbacks of the first version: reliance on a manually operated microscope and ~30 min per spectrum. Modularity let components to be upgraded and the platform to be adapted to other chips or combined with other techniques (optical tweezers, electroporation) [3].

CONCLUSIONS

OpenDEP is evolving from a microscope-attached lab-on-a-chip into a modular, open-source stand-alone instrument for acquiring DEP spectra and extracting cell dielectric parameters. With Control, Compute and View covering the workflow from acquisition to analysis and visualization, the platform offers laboratories a low-cost, reproducible alternative to commercial DEP systems.

ACKNOWLEDGMENT

This work was partially supported by a grant of the Ministry of Education and Research, CCCDI-UEFISCDI, project number PN-IV-PCB-RO-MD-2024-0285, within PNCDI IV, grant No 62PCBROMD/2025.

REFERENCES

[1] Tivig I. C., *et al.* doi: 10.1021/acsomega.3c06052, 2023.
[2] Yadav D. S., *et al.* doi.org/10.1186/s12886-024-03617-0, 2024.
[3] Gherghinoiu F., *et al.* doi.org/10.1021/acsomega.5c06195, 2025.
[4] Tivig I. C., *et al.* doi.org/10.1038/s41598-024-54350-z, 2024.

Breaking the bone barrier: electrochemotherapy for bone tumours in dogs and cats, a review

Lora Koenhemsi[1]; [1]*Department of Internal Medicine, Faculty of Veterinary Medicine, Istanbul University-Cerrahpaşa, Avcılar, 34320 Istanbul, TURKEY*

INTRODUCTION

Osteosarcoma (OS) is the most common primary bone tumour in dogs and one of the most frequent primary bone tumours in humans; the dog is therefore a natural model of the human disease [1,2]. Local control of bone tumours is difficult. Surgery and radiotherapy may not be possible in advanced disease or at complex sites, and OS cell membranes are thought to lack drug transport proteins, so drug uptake is low; high-dose chemotherapy has not solved this problem [2].

Electrochemotherapy (ECT) may help. Bleomycin (BLM) enters cells poorly, but electric pulses raise its uptake sharply [2,3]. Unlike radiotherapy and thermal ablation, ECT does not cause bone necrosis or weaken bone [3]. In mice with human OS xenografts, BLM plus electric pulses reduced tumour volume to 0.023 times baseline by day 14, while control tumours grew 2.3–3.2 times [2]. This review summarises the clinical evidence on ECT for bone tumours in dogs and cats and its main technical limits.

METHODS

Published case reports, case series and preclinical studies on ECT of bone tumours in dogs and cats were reviewed. Human clinical data on bone metastases and experimental studies on electrode design were included for comparison.

RESULTS

Protocol. In the reported cases, BLM (15,000 IU/m^2) was given intravenously under general anaesthesia, and eight 100 µs pulses were delivered about 8 minutes later [1,3]. Besides higher drug uptake, ECT causes vascular shutdown and immunogenic cell death [3].

Canine OS of the skull. The first canine OS treated with ECT was in a 13-year-old German Shepherd with a parietal bone tumour of about 5.5 × 8 cm [1]. After debulking, about 1 mm of tumour remained over the bone. Two adjuvant ECT sessions were given with needle electrodes (8 pulses of 100 µs at 5 kHz), together with five carboplatin sessions. The tumour recurred and a second ECT was given at 16 months; after this, there was no recurrence over 114 weeks and quality of life was good. Needle electrodes probably missed micro-infiltrates in trabecular bone. With plate electrodes and conductive gel in direct contact with bone, all skull layers were covered, and peak brain current density (about 2 A/cm^2) stayed far below the reported damage level [1].

Canine OS of a long bone. Bone-targeted ECT was used in a 12-year-old Akita with a 12 cm osteolytic OS of the proximal humerus [3]. A single-needle bipolar electrode was inserted through the cortex with a coaxial bone introducer (8 pulses, 100 µs, 1 kHz, 800 V; about 5 mm treatment radius per insertion). Six carboplatin doses followed. Pain control improved mildly; the dog stayed ambulatory, had no pathological fracture or pulmonary metastasis on available imaging, and was alive 37 weeks after diagnosis.

Cats. In the same series, three cats with oral squamous cell carcinoma invading the maxilla received one or two bone-targeted sessions [3]. The electrode could be passed through osteolytic bone, but benefit was palliative and short: all three cats died or were euthanised within 22 weeks.

Other evidence. A dog with recurrent multilobular tumour of bone of the rostral maxilla reached complete remission after ECT and was disease-free for about 12 months before late recurrence and metastasis. In 67 dogs with oral melanoma, absence of bone involvement was linked to longer time to progression and survival after ECT [3]. In humans with bone metastases, a systematic review of 8 studies (246 patients) reported complete response in 12%, partial response in 26.1% and stable disease in 55.5%; mean pain score fell from 6.9 to 2.7 [4].

Electrode design. Surface electrodes reach only a few millimetres into bone [1,3]. A coaxial bipolar needle electrode treats a zone of about 10 mm [5]; in ovine vertebrae it produced an 11.2 mm zone, and the spinal cord remained normal [6].

CONCLUSIONS

Evidence on ECT for bone tumours in dogs and cats is limited to a few case reports, one small case series and preclinical studies. The canine cases suggest that long-term local control is possible, while results in cats with bone-invading oral squamous cell carcinoma were only palliative. Electrodes that reliably electroporate bone, including trabecular bone, need to be developed, and prospective studies are needed to define patient selection, protocols and outcomes.

REFERENCES

[1] Martins Taques M., *et al*. Adjuvant electrochemotherapy after debulking in canine bone osteosarcoma infiltration. *Artif Organs*, 45:309-315, 2021.

[2] Ishikawa A., *et al*. Efficacy of electrochemotherapy with bleomycin to the murine osteosarcoma model. *Yamagata Med J*, 33:9-15, 2015.

[3] Zanasi A., *et al*. Feasibility of bone-targeted electrochemotherapy for palliation of bone tumors in dogs and cats. *J Am Vet Med Assoc*, 2026.

[4] Bocchi M. B., *et al*. Electrochemotherapy in the treatment of bone metastases: a systematic review. *J Clin Med*, 12:6150, 2023.

[5] Merola G., *et al*. Design and characterization of a minimally invasive bipolar electrode for electroporation. *Biology (Basel)*, 9:303, 2020.

[6] Salamanna F., *et al*. Application of a new coaxial bipolar electrode for the treatment of vertebral metastases: a pilot study in an ovine model. *Front Med (Lausanne)*, 12:1627296, 2025.

Pulsed electric field–induced hemolysis in human blood ex vivo

Luka Čemažar[1,2], Matej Reberšek[3], Matevž Škerget[1,2]; [1]*Faculty of Medicine, University of Ljubljana, 1000 Ljubljana, SLOVENIA;* [2]*Department of Hematology, University Medical Centre Ljubljana, SLOVENIA;* [3]*Faculty of Electrical Engineering, University of Ljubljana, Tržaška 25, SI-1000 Ljubljana, SLOVENIA*

INTRODUCTION

With the increasing use of electroporation in clinical practice, reports have emerged describing intravascular hemolysis as a direct consequence of erythrocyte membrane injury [1]. Published studies report varying incidence rates, most likely attributable to differences in the technologies employed, including electrode configuration and exposure duration. Nevertheless, some authors have described elevated laboratory markers of hemolysis in up to 95% of treated patients [2]. Although clinically significant complications are uncommon, substantial hemolysis may result in acute kidney injury secondary to free haemoglobin(Hb) release, hemoglobinuria, and renal tubular toxicity [3].

Further evidence comes from vitro study by Fišerová et al., in which blood samples exposed to electroporation demonstrated a field strength-dependent increase in hemolysis.. A significant increase was detected at field strengths of 1000 V/cm and above, with free Hb concentrations reaching 0.32 ± 0.16 g/L at 1000 V/cm and 2.2 ± 0.96 g/L at 1250 V/cm ($p < 0.01$), indicating direct electroporation-induced disruption of erythrocyte membrane integrity [4]. We therefore aimed to characterize the exposure threshold for erythrocyte hemolysis and the associated changes in routine hematologic parameters in human blood ex vivo

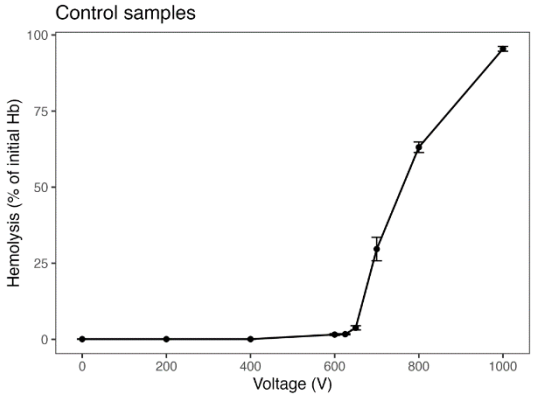
METHODS

An ex vivo experimental study was conducted on 10 healthy individuals using whole-blood samples tested in 800-µL electroporation 4-mm-gap cuvettes. Samples were exposed to different voltage levels 200, 400, 600, 625, 650, 700, 750, 800, and 1000 V. Following electroporation, samples were processed according to a standardized protocol and analyzed for markers of erythrocyte injury and hemolysis. Plasma Hb concentration was measured spectrophotometrically (expressed as percentage relative to the base line), while hematological parameters, including erythrocyte count, mean corpuscular volume (MCV), red cell distribution width (RDW), and platelet count, were determined using an automated hematology analyzer.

RESULTS

Hemolysis increased progressively with increasing applied voltage, showing a typical sigmoidal response pattern. At low voltages (0–400 V), hemolysis was negligible, remaining at approximately 0.1% across all measurements. A slight increase was observed at 600 V (1.6%), followed by a gradual rise at 625 V (2.2%) and 650 V (3.8%). A marked increase in hemolysis occurred between 650 V and 800 V. Mean % of initial Hb reached 29.7% at 700 V and increased further to 63.1% at 800 V. At the highest tested voltage (1000 V), hemolysis reached 95.5%. Hematological parameters remained largely unchanged up to 650 V, with stable MCV, platelet, RBC, and Hb values. Above 650 V, coinciding with the voltage range associated with substantial hemolysis, MCV increased, platelet-channel counts rose sharply, RBC counts progressively declined, and Hb concentrations remained relatively stable as expected.

Figure 1: Plasma Hb expressed as a percentage of the initial whole-blood Hb concentration, calculated as (plasma Hb concentration / initial whole-blood Hb concentration).



CONCLUSIONS

Overall, these findings demonstrate a strong voltage-dependent increase in erythrocyte hemolysis in healthy donors with the transition from minimal to substantial hemolysis occurring between 650 and 800 V and near-complete hemolysis observed at 1000 V. The observed changes (RDW, RBC, MCV etc.) are consistent with a sequence of erythrocyte swelling and fragmentation preceding extensive hemolysis. Rising MCV with preserved RBC counts was followed by the sharp increase in platelet counts (counting all fragments/artefacts/debris) coincided with the inflection point of the hemolysis curve, suggesting that fragmentation is an intermediate step in electric-field-induced erythrocyte destruction.

REFERENCES

[1] Zhou M., *et al.* Pulse field ablation: an update on energy-specific adverse events. *Rev Cardiovasc Med*, 26:44442, 2025.

[2] Koh T.W.Y., *et al.* Intravascular haemolysis following pulsed field ablation pulmonary vein isolation for atrial fibrillation: a systematic review. *Open Heart*, 12:e003684, 2025.

[3] Miyajima K., *et al.* Hemolysis and renal tubular injury after pulsed field ablation: A comparison between two commercially available platforms. *Heart Rhythm*, 2026.

[4] Fiserova I., *et al.* Significant hemolysis is present during irreversible electroporation of cardiomyocytes in vitro. *Heart Rhythm*, 22:466–474, 2025.

Electric field distribution in a full porcine torso geometry with varying return electrode placement in cardiac PFA: a computational model

Luca Pasini[1], Gerard Amorós-Figueras[2], Zoraida Moreno Weidmann[2], David Viladés Medel[2], Aurel Neic[3], Edward J. Vigmond[4,5], Antoni Ivorra[6], Jose M. Guerra[2], Luca Gerardo-Giorda[1,7], Argyrios Petras[1]; *[1]Johann Radon Institute for Computational and Applied Mathematics , Austrian Academy of Sciences, Linz, AUSTRIA; [2]Department of Cardiology, Hospital de la Santa Creu i Sant Pau, IR SANT PAU, Universitat Autònoma de Barcelona, Barcelona, SPAIN; [3]NumeriCor GmbH, Graz, AUSTRIA; [4]Liryc Heart Rhythm Disease Institute, Fondation Bordeaux University, Bordeaux, FRANCE; [5]CNRS, Bordeaux INP, IMB, University of Bordeaux, Bordeaux, FRANCE; [6]Department of Engineering, Universitat Pompeu Fabra, Barcelona, SPAIN; [7]Institute for Mathematical Methods in Medicine and Data-Based Modelling, Johannes Kepler University, Linz, AUSTRIA*

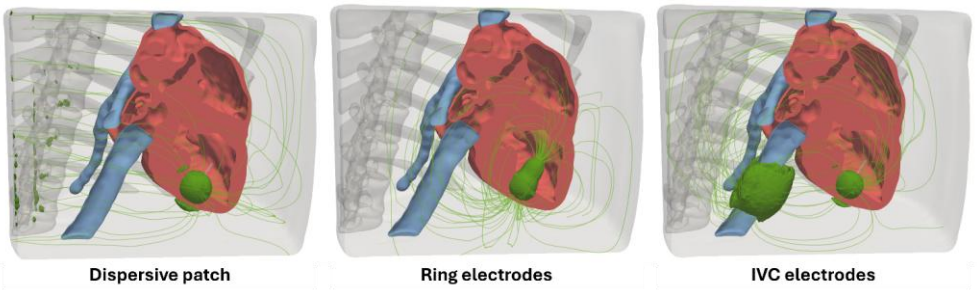


Figure 1: Electric field distribution in the torso for the three investigated configurations. Green lines represent the electric field streamlines, while the highlighted green regions indicate where the electric field exceeds the 100 V/cm threshold.

INTRODUCTION

Pulsed field ablation (PFA) is an emerging cardiac ablation technique that uses short, high-voltage electrical pulses to induce myocardial lesions through cellular electroporation. Preclinical studies have repeatedly investigated strategies to increase lesion depth by varying catheter positioning and electrode design, both of which are recognized as key determinants of lesion formation. In this work, we investigate the effect of different return electrode configurations on lesion formation and on the resulting electric field distribution, using a computational model of a full-torso porcine geometry.

METHODS

The full 3D porcine geometry previously reconstructed by our group [1] is adopted in this study. Myocardial fiber orientation is introduced within the ventricular wall using a rule-based method. A point-by-point catheter is positioned at the endocardial left ventricular wall, accounting for the cardiac wall deformation resulting from the application of a 20 g contact force.

Three different return electrode configurations (0 V) are investigated: (i) a dispersive patch positioned on the dorsal side of the animal; (ii) three 2 mm ring electrodes positioned along the catheter shaft; and (iii) a second catheter positioned in the inferior vena cava (IVC). A voltage of 1000 V is applied to the active electrode.

The electric field distribution is computed accounting for the increase in electrical conductivity induced by electroporation, the relative orientation between the electric field and the cardiomyocytes, and the reduced effect of electroporation along the fiber direction due to gap junctions [2].

RESULTS

Similar lesion shapes and dimensions are observed for the ring electrode and dispersive patch configurations, whereas the IVC configuration produces shallower lesions.

Analysis of the electric field distribution throughout the full torso shows that the dispersive patch configuration produces a stronger electric field across a larger portion of the torso, with high field values also far from the active electrode, in the vicinity of the patch. In contrast, the IVC configuration results in a focalized electric field in the active catheter region, with a second high intensity region near the return catheter in the IVC. The ring electrode configuration results in the most focalized field (Figure 1).

CONCLUSIONS

The proposed computational model addresses the effect of return electrode configuration on lesion dimensions and electric field distribution across a full torso geometry. The results highlight the importance of return electrode placement in determining the spatial distribution and localization of the electric field throughout the torso, while it has a smaller impact on the final lesion dimensions.

REFERENCES

[1] Petras A., *et al*. Is a single lethal electric field threshold sufficient to characterize the lesion size in computational modeling of cardiac pulsed-field ablation? *Heart Rhythm O2*, 6:671-677, 2025.

[2] Petras A., *et al*. Competing mechanism in monopolar cardiac PFA can reproduce experimentally observed asymmetric lesions. *Card Eng Tech*, *Under Review*

Integrated dielectrophoresis and optical tweezers for single-cell characterization

Florela Gherghinoiu[1], Ioan Tivig[1], Mihaela G. Moisescu[1], Tudor Savopol[1]; [1]*Biophysics and Cellular Biotechnology Department, Faculty of Medicine, "Carol Davila" University of Medicine and Pharmacy, Bucharest, ROMANIA*

INTRODUCTION

Understanding living cells in their physiological state requires non-invasive, label-free approaches that capture cell-to-cell heterogeneity. Single-cell methods enable the characterization of individual cellular properties and dynamic responses that can be masked by population-based measurements. Here, we combine dielectrophoresis (DEP) and optical tweezers (OT) to noninvasively determine both DEP spectra and optical trap stiffness on the same living cell.

METHODS

The experimental setup consisted of a custom-fabricated DEP chip incorporating a DEP chamber with two electrode configurations, band and triangular, integrated with a 1064 nm laser-based optical tweezers system on an inverted microscope. Electric-field intensity and gradient distributions were characterized by numerical simulations for both electrode geometries. NIH3T3 cells were first characterized by population-based DEP and subsequently by single-cell DEP-OT measurements. DEP measurements were performed in sucrose-based buffers with controlled conductivity, covering the range of 0.02-0.08 S/m.

For single-cell analysis, individual cells were optically trapped within the DEP chamber and exposed to the same frequency range used for population measurements (5 KHz-50 MHz, 10 Vpp). Cell displacement under the applied DEP field was recorded by image-based analysis and used to determine the cell-specific DEP response and relative DEP spectra. The electrical parameters obtained from the DEP spectrum were then used to calculate the DEP force acting on the same optically trapped cell.

By measuring the corresponding cell displacement, the DEP force-displacement relationship was used to determine the optical trap stiffness, enabling direct on-cell calibration of OT stiffness. The DEP-derived stiffness was independently validated using the hydrodynamic drag-force method. OpenDEP [1] was used for automated image-based analysis and extraction of relative DEP spectra, cellular electrical parameters, and OT stiffness. Cell viability was assessed by MTS assay to verify non-invasive experimental conditions.

RESULTS

Single-cell DEP spectra reproduced the overall trends observed in population measurements while revealing cell-to-cell heterogeneity and enabling repeated characterization of the same cell. OT stiffness determined using the two electrode geometries tested showed consistent values and agreed in order of magnitude with the independent drag-force method, supporting direct on-cell OT calibration.

Increasing buffer conductivity (0.02-0.08 S/m) shifted the DEP spectra and was accompanied by a clear increase in OT stiffness. This trend is attributed primarily to the lower sucrose concentration and consequently lower refractive index of higher-conductivity buffers, which increases the refractive-index contrast between the cell and surrounding medium and thus enhances the optical gradient force. Cell viability remained above 80%, with no significant reduction after exposure for up to 15 min. Across the tested laser powers (27, 31.5, and 36 mW), the DEP spectra and first and second crossover frequencies remained highly consistent, confirming that DEP measurements were independent of trapping power within the stable trapping regime. OT stiffness showed only a slight, non-significant increase with laser power [2].

CONCLUSIONS

By combining both DEP and OT, the proposed method enables direct determination of DEP-derived electrical parameters and OT stiffness from the same living cell. In particular, it allows direct on-cell calibration of OT stiffness on the cell of interest, providing cell-specific electrical and optical measurements within a unified experiment. The consistent performance across the tested conditions supports the applicability of the method for single-cell biophysical characterization.

ACKNOWLEDGMENT

This work was partially supported by a grant of the Ministry of Education and Research, CCCDI-UEFISCDI, project number PN-IV-PCB-RO-MD-2024-0285, within PNCDI IV, grant No 62PCBROMD/2025.

REFERENCES

[1] Tivig I., *et al*. OpenDEP: An open-source platform for dielectrophoresis spectra acquisition and analysis. *ACS Omega*, 8:38715-38722, 2023.

[2] Gherghinoiu F., *et al.* All-in-one method for iterative single-cell dielectrophoretic and optical characterization: advancing the OpenDEP platform. *ACS Omega*, 10:44333-44343, 2025.

Electric field strength shifts protein responses from thermal-state dependence toward structure-guided remodeling

NeNe Yoshioka[1], Sho Mawatari[1], Sunao Katsuki[2]; *[1]Graduate School of Science and Technology, Kumamoto University, Japan [2]; Institute of Industrial Nanomaterials, Kumamoto University, JAPAN*

INTRODUCTION

PEF treatments are often optimized empirically despite involving multiple physical mechanisms [1]. Toward mechanism-based pulse design, we investigated the direct electric field effect on ovalbumin using sub-nanosecond PEF experiments and atomistic molecular dynamics simulations [2].

METHODS

OVA was exposed to 100 shots of 0.7-ns electrical pulses at 50–150 MV/m under conditions designed to minimize thermal and electrochemical effects. Structural changes were assessed using area-normalized UV second-derivative spectroscopy. Atomistic MD simulations were performed at 300 K using AMBER99SB-ILDN/TIP3P with 0.15 M NaCl under fields of 0.1–1.0 V/nm, and local turnover and RMSF were analyzed to separate spontaneous dynamics from field-specific remodeling.

RESULTS AND DISCUSSION

The UV second-derivative spectra showed minor changes at 50–100 MV/m but a clearer alteration of the aromatic absorption band at 150 MV/m, which persisted after area normalization (Figure 1). To examine the molecular origin of this experimentally observed response, MD trajectories at the corresponding field strength of 0.15 V/nm were analyzed.

At 0.15 V/nm, field-induced local turnover was strongly correlated with spontaneous local turnover (Spearman $\rho = 0.792$; Figure 2), indicating that the response observed at this field largely followed thermally accessible local dynamics rather than a distinct remodeling pathway.

We then extended the MD analysis to 0.1–1.0 V/nm to determine how this response changed with the field strength. Increasing the field strength shifted excess remodeling toward intrinsically flexible sites while reducing trajectory-state dependence (site RMSF × field: $\beta = 0.0409$, $p = 1 \times 10^{-5}$; trajectory RMSF × field: $\beta = -0.0239$, $p = 0.0083$). At 1.0 V/nm, site flexibility was positively associated with excess remodeling ($\rho = 0.402$; Figure 3).

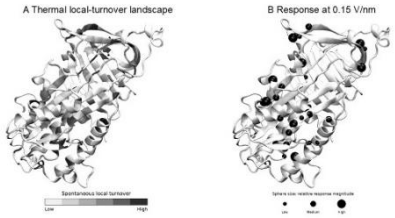


Figure 2: Spontaneous local turnover and low-field response at 0.15 V/nm.

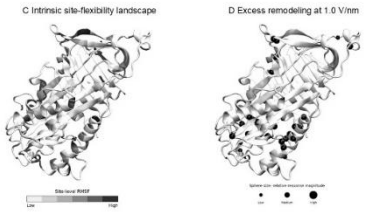


Figure 3: Intrinsic site flexibility and excess remodeling at 1.0 V/nm.

CONCLUSION

These results indicate that the direct structural response of OVA changes with electric field strength: low-field responses largely follow thermally accessible local dynamics, whereas stronger fields increasingly promote remodeling at intrinsically susceptible sites. This field-dependent change in response determinants and affected regions suggests that appropriate pulse parameters may enable more selective structural modification of proteins, supporting mechanism-based PEF design.

REFERENCES

[1] Kotnik T., *et al.* doi: 10.1146/annurev-biophys-052118-115451.

[2] Cifra M., *et al.* doi: 10.1039/d3cs00244f.

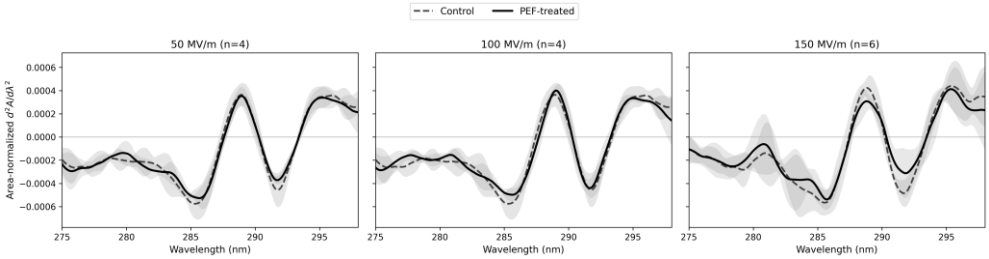


Figure 1: Area-normalized second-derivative UV spectra of OVA after PEF treatment.

Annexin A4 relocalisation and plasma membrane stabilisation in response to electroporation

Haroldas Sakavičius[1], Baltramiejus Jakštys[1], Saulius Šatkauskas[1]; [1] *Faculty of Natural Sciences, Vytautas Magnus University, Universiteto g. 10, Akademija, Kauno raj. sav., LT-53361, LITHUANIA*

INTRODUCTION

Electroporation (EP) is a technique used to transiently permeabilize the plasma membrane, but it imposes a critical need for rapid cellular repair [1]. Annexin A4 (ANXA4), a calcium-binding protein, is a key component in membrane resealing, yet its dynamics during electrically induced disruption are not fully understood [2].

This study investigates the spatiotemporal redistribution of ANXA4 following electroporation to determine how pulse parameters and extracellular calcium influence the repair process.

METHODS

Wild-type and ANXA4-knockout (KO) MCF-7 cells were exposed to single 100 µs square-wave pulses across a range of field strengths (0.8–3.6 kV/cm). Experiments were performed in iso-osmotic HEPES buffer, either supplemented with 2 mM $CaCl_2$ or without added $CaCl_2$. The redistribution of ANXA4-GFP was monitored using live-cell fluorescence microscopy, while cell viability and membrane resealing were quantified through MTS assays and propidium iodide (PI) uptake using flow cytometry.

RESULTS

The study showed that extracellular calcium enhanced ANXA4 membrane recruitment, producing faster and stronger ANXA4 translocation. In calcium-free conditions, ANXA4 remained predominantly diffuse in the cytosol and showed only weak or delayed membrane recruitment, whereas calcium supplementation induced rapid and robust translocation to the membrane, scaling with pulse strength. Quantitative analysis showed that in Ca^{2+}-supplemented conditions, field strengths ≥1600 V/cm accelerated recruitment kinetics and increased cortical intensity. Furthermore, ANXA4 preferentially accumulated at electrode-facing poles, mirroring theoretical permeabilization patterns. KO cells exhibited significantly impaired resealing and higher mortality in calcium-supplemented medium, supporting a key role for ANXA4 in post-pulse survival.

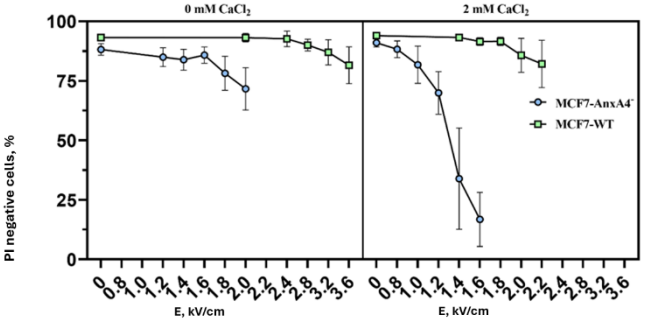


Figure 1: Assessment of plasma membrane repair via PI exclusion (dye added 35 min post-electroporation).

CONCLUSION

Our findings identify ANXA4 as a precise responder to electroporation-induced injury, linking extracellular Ca^{2+} availability and ANXA4 recruitment with stabilization of permeabilized membrane domains. The results demonstrate that pulse parameters and calcium availability strongly modulate the efficiency of the repair response. These insights provide a biophysical basis for optimizing electroporation-based protocols by balancing membrane permeabilization, repair, and cell survival according to the intended application.

REFERENCES

[1] Mahnič-Kalamiza S., *et al.* Electroporation in food processing and biorefinery. *J Membr Biol*, 247:1279–1304, 2014.

[2] Boye T. L., *et al.* Annexin A4 and A6 induce membrane curvature and constriction during cell membrane repair. *Nat Commun*, 8:1–11, 2017.

Mathematical modeling of the membrane of a cell using the Cahn Hilliard PDE

Mahé Ambert*; Centre INRIA de Rennes, Université de Rennes, FRANCE*

INTRODUCTION

When an electric field is applied to the membrane of a cell, it becomes more permeable. This phenomenon is called electroporation. The purpose of my PhD will be to understand electroporation from a mathematical standpoint using PDEs at a microscopic level, but for now I am modeling the membrane of a cell before any electric field is applied.

MODEL

The membrane of cells are lipid bilayers. Lipids are amphiphilic molecules, which mean that when plunged in water they tend to self organize. For example, if one tries to mix water with oil, after a short period of time the two liquids will separate themselves, forming two phases. The PDE that I will be using to model this is the following:

Equation 1: Cahn – Hilliard equation

$$\begin{cases} \partial_t u = \Delta \mu \\ \mu = f(u) - \varepsilon^2 \Delta u \end{cases}$$

The solution u is a local concentration, its value is 1 if there is only water and -1 if there is only lipids. μ is the chemical potential, ε is a characteristic length of the problem, and f is the derivative of a double-well potential W that has 1 and -1 as its minima. The energy associated with this equation is minimized when the interface (the region where u=0, which exists since u is continuous) between the phase u=1 and the phase u=-1 is as small as possible.

As seen on figure 1, starting from a random u close to 0, the two phases separate themselves pretty quickly and then the system stabilizes towards a stripe, which minimizes the interface.

ASYMPTOTIC EXPANSION

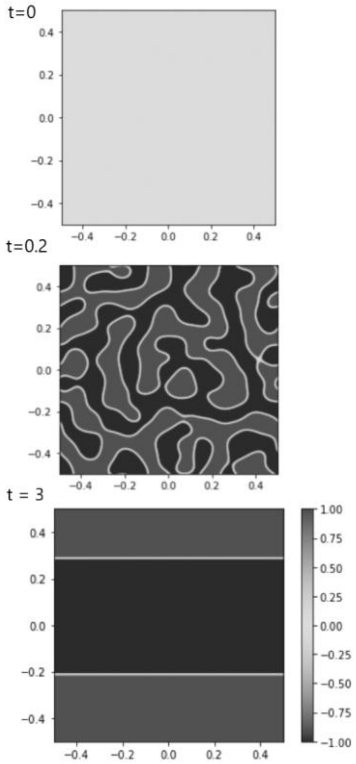
To better understand the geometric properties of the interface between the two phases, and especially how it moves in order to reach the minimal configuration, we introduce a function d(x,t) which measures the shortest distance between the point x (in n dimensions) and the interface at time t. We can then assume that the function u is of the form u(x,t,d(x,t)/ε) and by doing a chain-rule and a substitution in the Cahn-Hilliard equation, we obtain a system of equations on the distance d, which is called Mullins-Sekerka. This method is inspired by [2].

Another equation called Allen Cahn can be used to describe the water/lipid situation. It is the same equation without the Laplacian in front of μ. When doing the asymptotics for Allen Cahn, the equation obtained on d is the mean curvature movement, which means the equilibrium is either going to be a circle or a stripe (in case of periodic boundaries on a finite domain). The Mullins Sekerka equations are more complex, but the advantage Cahn Hilliard has over Allen Cahn is that the mass is conserved, which is a reasonable property.

RESULTS AND FIGURES

Since f is non-linear (typically u^3 – u), creating a stable numerical scheme to approximate a solution of Cahn-Hilliard can be quite challenging. An idea of a method is given in [3]. We decompose the energy in two parts, one convex and one concave and then we explicit the concave part and implicit the convex part.

Figure 1: Evolution of u



On this figure one can see the concentration u(t,x,y) for different times. The domain is the square [-0.5,0.5]^2, with periodic boundary conditions. The grayscale indicates the values of u on the square (see the colorbar next to the t=3 figure). At t=0 we start from u being a random noise very close to 0, which physically means the water and the lipids are mixed together. At t=0.2 we can see a phenomenon called "spinodal decomposition", where zones appear. In these zones u is either equal to 1 or -1, which means there is either only lipids or only water. At t=3, the zones moved and stabilized into a position where the interface between them is minimal.

REFERENCES

[1] Mahé A., Under the direction of Clair Poignard,masters degree internship report, Cahn-Hilliard equation and electroporation, 2026

[2] Robert L. P., Front migration in the nonlinear Cahn-Hilliard equation, *The Royal Society* , 1988.

[3] Huailing S., Energy SSP-IMEX Runge–Kutta methods for the Cahn–Hilliard equation, *J Comput Appl Math*, 292: 576-590, 2016

Effect of specific energy input on pilot-scale PEF inactivation and post-treatment survival of a beer spoilage yeast

Sanja Ludoški[1], Dagbjørn Skipnes[2], Martin Watson[2], Torstein Skåra[2], Dmytro S. Kozak[1], Monika Polańska[1], Simen Akkermans[1], Jan F.M. Van Impe[1]; *[1]BioTeC+ - Chemical and Biochemical Process Technology and Control, KU Leuven, Gebroeders de Smetstraat 1, 9000 Gent, BELGIUM; [2]Department of Processing Technology, Nofima AS, P.O. Box 8034, NO-4068, Stavanger, NORWAY*

INTRODUCTION

Non-alcoholic beer (NAB) is currently the fastest-growing category of the beer market [1]. Compared to alcoholic beer, the presence of residual sugars combined with a low ethanol content (0–0.5%) leaves it more susceptible to microbial spoilage. Thermal pasteurisation remains the standard for ensuring microbial safety, but it negatively affects the sensory quality and increases energy demand [2]. This trade-off has driven growing interest in non-thermal preservation techniques capable of achieving adequate microbial inactivation without compromising product quality. Pulsed electric field (PEF) processing applies short (1–10 µs), high-voltage (20–80 kV/cm) electrical pulses to induce electroporation in microbial cells, disrupting their membranes and causing inactivation [3]. Although earlier studies have demonstrated the potential of PEF for beer preservation, inconsistencies in processing parameters and a limited amount of pilot-scale research make it difficult to draw firm conclusions regarding the efficacy of microbial inactivation [4, 5, 6].

The aim of this study was to evaluate the effect of increasing specific energy inputs on the inactivation of a beer-relevant spoilage yeast in a simplified malt extract model-liquid, providing a controlled matrix representative of NAB.

MATERIALS AND METHODS

Experiments were conducted in a PEF Pilot Dual system (Elea GmbH, Quakenbrück, Germany) with a DN10-10 colinear continuous-flow cell. A volume of 50 L of model-liquid, consisting of malt extract dissolved in water (40 g/L) was inoculated with *Saccharomyces cerevisiae* subsp. *diastaticus* (1×10^6 CFU/mL) isolated from super-attenuated beer (DSM 70487, Leibniz Institute DSMZ-German Collection of Microorganisms and Cell Cultures). Electric field strength and pulse width remained constant (24 kV/cm; 8 µs) at a flow rate of 130 L/h. Four increasing intensities of specific energy (W_{spec}) were tested (10, 15, 25, 35 kJ/L). After treatment samples were stored at 4°C and 22°C and plated at multiple time points during a period of two weeks, to determine whether there will be microbial regrowth or further inactivation of the target spoiler.

RESULTS AND FIGURES

Increasing W_{spec} resulted in increased microbial inactivation (Table 1), ranging from 0.82 log reduction at 10 kJ/L to 2.15 log reduction at the highest tested specific energy input of 35 kJ/L.

Table 1: PEF-induced log reduction.

W_{spec}(kJ/L)	Log Reduction	SD
10	0.82	0.13
15	0.74	0.64
25	1.68	0.62
35	2.15	0.18

Substantial microbial regrowth (1.8-3.5 log CFU/ml increase) was noted at the end of the two-week storage period in the samples stored at 22°C, with counts reaching approximately 7 log CFU/ml by day 10, regardless of the applied W_{spec}. Refrigerated samples showed limited regrowth of 0.1-0.5 log CFU/ml after two weeks of storage, compared to post-treatment counts. These results demonstrate the importance of storage temperature in controlling post-treatment microbial growth.

CONCLUSION

Although the results showed that microbial inactivation by PEF was dependent on the applied W_{spec}, the tested conditions caused limited inactivation while surviving cells showed regrowth during storage at 22°C. In future, the effects of changes in other processing parameters as well as the application of higher specific energy inputs on microbial inactivation will be studied, which may result in greater microbial inactivation and enhance storage stability.

REFERENCES

[1] The Brewers of Europe, 'European Beer Trends Statistics Report | 2025 Edition', 2025.

[2] Roselli G. E., *et al*. The two faces of microorganisms in traditional brewing and the implications for no- and low-alcohol beers. *Front Microbiol*, 15: 1346724, 2024.

[3] Mosqueda-Melgar J., *et al*. Effects of pulsed electric fields on pathogenic microorganisms of major concern in fluid foods: a review. *Crit Rev Food Sci Nutr*, 48:747–759, 2008.

[4] Milani E. A., *et al*. Pulsed electric field continuous pasteurization of different types of beers. *Food Control*, 50:223–229, 2015.

[5] Ulmer H. M., *et al*. Effects of pulsed electric fields on inactivation and metabolic activity of Lactobacillus plantarum in model beer. *J Appl Microbiol*, 93: 326–335, 2002.

[6] Evrendilek G. A., *et al*. Pulsed electric field processing of beer: Microbial, sensory, and quality analyses. *J Food Sci*, 69: M228–M232, 2004.

Electroporation-based sampling of live tissue for spatiotemporal omics

Chantelle Spiteri[1], Ciro Chiappini[1]; [1]*Centre for Craniofacial and Regenerative Biology, King's College London, London, UNITED KINGDOM*

INTRODUCTION

Spatially resolved molecular analysis of intact tissues is essential for understanding how cellular processes are organised within their native tissue environment [1]. However, conventional molecular profiling approaches often require tissue disruption or fixation, limiting the ability to preserve spatial information and interrogate dynamic molecular processes.

Recent studies have demonstrated that biomolecules can be sampled from living tissue while preserving spatial information and tissue viability. This enables longitudinal mapping of tissue lipidomics and other molecular profiles, as demonstrated by repeated spatial lipidomic profiling of living brain tissue using porous silicon nanoneedles [2]. These approaches rely on direct nanoneedle–tissue contact to collect biomolecules. In parallel, electroporation has emerged as a means of enabling controlled molecular exchange through transient membrane permeabilisation, including intracellular sampling using nanostructured interfaces [3,4].

Building on these approaches, we are developing a tissue-scale electroporation platform for spatially resolved molecular sampling from brain tissue. The platform incorporates a 3D-printed tissue–electrode interface that enables controlled positioning of tissue between the electrodes and a molecular collection substrate, providing a defined architecture for electroporation and molecular transfer. Using this system, we demonstrate spatially resolved protein transfer from brain tissue while maintaining tissue viability under the electroporation conditions tested. The approach is further compatible with mass spectrometry imaging, providing a route towards spatial analysis of transferred biomolecules.

By combining controlled electroporation, tissue–electrode engineering and substrate-based molecular capture, this platform provides a foundation for minimally disruptive molecular sampling from intact tissue. The approach could enable complementary proteomic and metabolomic analysis while preserving the anatomical information of the sampled tissue, supporting the development of longitudinal molecular interrogation of living tissue.

METHOD

Brain Tissue Preparation and Electroporation. Mouse brains were sectioned at 250 µm thickness using a vibratome. Tissue sections were transferred onto the holder and incubated for 24 h prior to electroporation. The following day, the tissue–membrane assembly was subjected to nano-electroporation using a range of electrical parameters, including voltage, pulse frequency and pulse duration, to evaluate their effects on molecular extraction.

Following electroporation, the collection substrate was used for downstream analysis. For protein detection, the substrates were analysed using Ponceau staining to assess the presence of protein transferred from the tissue. The brain tissue after electroporation was stained for live dead to determine if the electroporation conditions are too harsh or if they are fine with viability. The brain tissue was also assessed using live/dead staining to evaluate tissue viability after electroporation.

RESULTS

The electroporation device developed consists of two sections: an upper component designed to securely position the brain tissue and a lower component supporting the collection substrate **(Figure 1a)**. This configuration positions the tissue between the electrodes and collection substrate. Live/dead staining following application of the selected electroporation conditions **(Figure 1b,c)** showed predominantly viable cells, with no substantial increase in cell death observed under the conditions tested. Ponceau staining of the collection substrate revealed protein transfer corresponding to the anatomical shape of the brain tissue **(Figure 1d).**

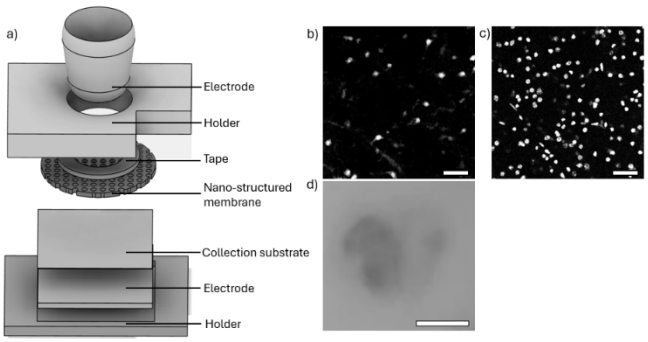


Figure 1: (a) Electroporation device. (b,c) Live/dead staining after electroporation: (b) dead cells (c) Hoechst-stained nuclei. (d) Ponceau staining. Scale bar: (b-c) 100µm, (d) 0.5cm.

CONCLUSION

The developed platform enables spatially resolved molecular transfer from brain tissue while maintaining tissue viability. This provides a foundation for further optimisation of electroporation-mediated molecular sampling and downstream spatial proteomic and metabolomic analysis.

REFERENCES

[1] Palla G., *et al*. Spatial components of molecular tissue biology. *Nat Biotechnol,* 40:308–318, 2022.

[2] Gu C., *et al*. Nanoneedles enable spatiotemporal lipidomics of living tissues. *Nat Nanotechnol*, 20:1262–1272, 2025.

[3] Quek Y. J., *et al*. Nanostraw electroporation for temporal RNA sampling from living 2D and 3D cell culture systems. *ACS Nano*, 19: 37847–37864, 2025.

[4] Tay A., *et al*. Transfection with nanostructure electro-injection is minimally perturbative. *Adv Ther*, 2:1900133, 2019.

Quantitative phase imaging as an intelligent label-free approach for biophysical analysis of cells and tissues

Mihaela G. Moisescu[1], Violeta L. Calin[1], Ioan Tivig[1], Christien O. Matei[1], Florela Gherghinoiu[1], Adrian V. Dumitru[1], Nicolae Tarba[2], Mona Mihailescu[2], Tudor Savopol[1]; *[1]Faculty of Medicine, Carol Davila University of Medicine and Pharmacy, Bucharest, ROMANIA; [2]Faculty of Applied Sciences, National University of Science and Technology Politehnica, Bucharest, ROMANIA*

INTRODUCTION

Quantitative Phase Microscopy (QPM) provides a label-free imaging technique for visualizing transparent samples (cells, tissues) and generates quantitative phase images (QPIs), in which each pixel encodes the phase shift induced by the specimen. The QPIs enable the extraction of phase-derived, geometrical, morphological, and textural parameters, providing objective information about cellular and tissue properties particularly those related to cellular protein content. When extracted from tissue sections and used as inputs to machine learning (ML) algorithms, these parameters can support the development of intelligent procedures for pathological tissue assessment and grading [1]. Such approaches hold promise as tools to assist pathologists in achieving more accurate diagnoses. Moreover, QPM showed capability in capturing information about cells underwent fast processes without any disturbance of cell status [2].

Here, we investigated QPM in two complementary applications: (I) real-time monitoring of the responses of adherent cells to electroporation (EP) and (II) intelligent assessment of colonic tissue samples.

MATERIALS AND METHODS

For study (I), DC3F fibroblasts were cultured on indium tin oxide (ITO)-coated glass coverslips and exposed to bipolar rectangular pulses of 400, 800, or 1000 V/cm. QPIs data were obtained using a SID4 HR camera (Phasics, France) in fast and slow time-lapse modes over a 20-min period, with reference images recorded before pulse delivery. Phase-derived parameters, together with geometrical, morphological, and textural features, were extracted and analyzed using laboratory-developed software integrated into ISHE platform. Successful electropermeabilization was confirmed by propidium iodide uptake.

For study (II), pairs of serial histological sections were prepared from colonic lymph nodes and adenomatous polyps exhibiting low- or high-grade dysplasia, following standard histopathological procedures. One section from each pair was H&E stained and evaluated by a pathologist, while the consecutive section was left unstained for QPIs acquisition using an off-axis digital holographic microscope (DHM®-T1000, Lyncée Tec, Switzerland). The samples are part of the HoloPath collection of colonic tissues.

RESULTS AND DISCUSSION

In study (I), electroporation produced significant changes in phase (Figure 1), GLCM-derived textural, and geometrical parameters, with the highest pulse voltage inducing the most pronounced modifications. During the first minute after EP, parameter changes rapidly approached a plateau, followed by slower variations during the subsequent monitoring period, while the membrane resealed or sustained irreversible disruption.

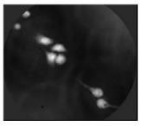


Figure 1: Example of QPIs of DC3F cells before (up) and 20-min after (down) pulse application showing internal phase redistribution.

In study (II), a digital library of QPIs and a workflow for colonic tissue analysis were established (Figure 2). Supervised machine-learning (ML) models classified lymph node superpixels as normal or invasive, achieving 97.91% sensitivity and 98.62% specificity and enabling the identification of suspicious regions [3]. The approach is being extended to colonic polyps using unsupervised algorithms for histological structure identification and supervised models for dysplasia grading and invasion mapping, targeting 90% overall accuracy. The HoloPath multimodal interface supports data annotation and model implementation.

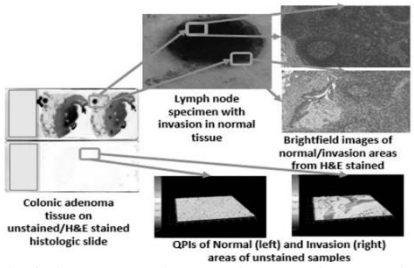


Figure 2: Schematic of procedure and examples of QPIs from Normal/Invasion areas of lymph nodes tissue [3].

CONCLUSIONS

QPM provides a versatile, non-invasive platform for biophysical characterization across different biological scales. Its ability to monitor real-time changes induced by electroporation, combined with the development of holographic biomarkers and intelligent image-analysis algorithms for colorectal tissue, supports its potential as a powerful tool for both experimental biophysics and computer-assisted pathology. The integration of quantitative phase information with automated image analysis contribute to objective, efficient, and reproducible assessment of cellular and tissue responses.

REFERENCES

[1] Calin L. V., *et al.* doi: 10.1016/j.heliyon.2024.e29897, 2024.
[2] Calin L. V., *et al.* doi: 10.1364/BOE.421959, 2021.
[3] Calin L. V., *et al.* doi: 10.1109/JPHOT.2025.3650039, 2026.

Computational analysis of peripheral nerve electroporation: fiber-type vulnerability and electric field effects

Berta Mateu[1], Antoni Ivorra[1] , [1]*Biomedical Electronics Research Group, Department of Engineering, Universitat Pompeu Fabra, Poblenou Campus, Barcelona, SPAIN*

INTRODUCTION

Electroporation is increasingly used in clinical applications, including cancer therapies, making it important to understand its effects on nearby peripheral nerves. Peripheral nerve fibers differ in their structure, particularly in myelination and axonal diameter, which may influence their susceptibility to externally applied electric fields. Myelin provides electrical insulation, potentially modifying the distribution of the electric field and the resulting membrane response. In this study, we first investigate how myelination and axonal diameter affect electroporation susceptibility. We then focus on myelinated axons to determine whether the nodes of Ranvier, due to their lack of myelin insulation, are more susceptible to electroporation than internodal regions, and whether non-uniform electric fields enhance electroporation compared with uniform fields.

MATERIALS AND METHODS

Peripheral nerve fibers were modeled using COMSOL Multiphysics. Representative fiber diameters were selected within physiological ranges: A fibers were modeled with diameters of 5.7, 8.7, 10, 14, and 16 μm, while C fibers were modeled with a diameter of 2 μm [1]. For myelinated fibers, nodes of Ranvier and internodal segments were explicitly represented to capture spatial heterogeneity in membrane exposure. Axons were exposed to uniform longitudinal and transverse electric fields of varying magnitudes under static simulation conditions. Additionally, a non-uniform electric field generated by two needle electrodes was evaluated for the 16 μm diameter fiber to investigate the response under a more spatially heterogeneous stimulation configuration.

Electroporation was assessed by modelling membrane conductivity increase due to transmembrane voltage as described in [2]. The relative pore area (RPA) [3] was computed for each membrane compartment to assess the degree of electroporation under each condition. Electroporation onset was defined as the minimum electric field strength at which the RPA reached 10^{-4} [3], following previously reported modelling criteria.

RESULTS

Preliminary results showed higher RPA for transverse than longitudinal electric fields. Myelinated fibers with different axonal radii exhibited similar electroporation dynamics under the same uniform field conditions, whereas unmyelinated fibers showed substantially lower RPA values (Figure 1). Within myelinated fibers, nodal regions exhibited higher RPA than internodal regions. Non-uniform electric fields produced higher RPA values at lower field magnitudes compared with uniform fields, indicating an increased electroporation response under spatially heterogeneous exposure (Figure 2).

CONCLUSIONS

Electroporation susceptibility was mainly influenced by myelination and electric field configuration, while axonal diameter had a limited effect. Nodes of Ranvier showed increased susceptibility compared with internodal regions. Non-uniform fields produced higher electroporation levels than uniform fields at low field magnitudes, suggesting a role of field spatial gradients.

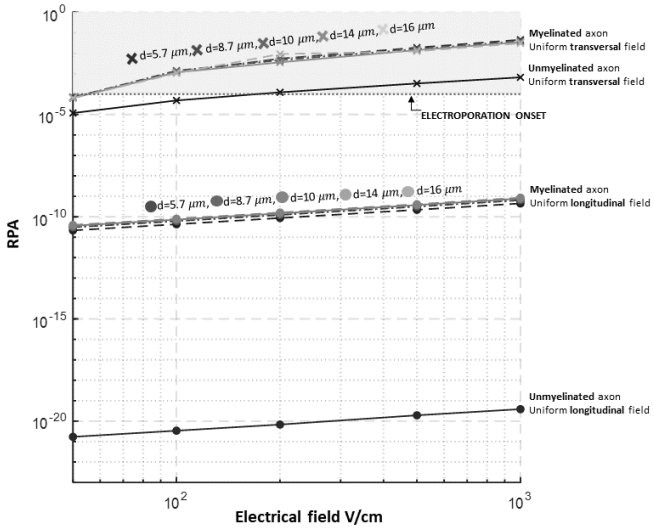


Figure 1: Maximum RPA for each electric field orientation and axon type.

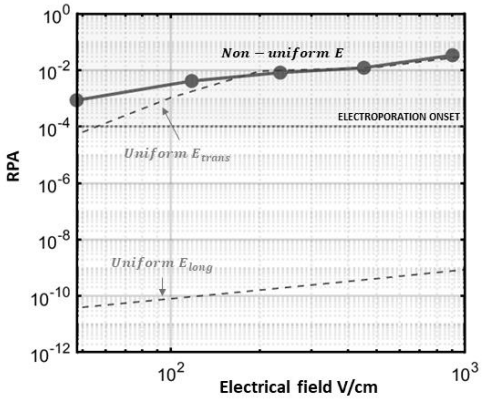


Figure 2: Maximum RPA for non-uniform electric versus uniform field electric fields in a 16 μm myelinated axon.

REFERENCES

[1] McIntyre C.C., *et al*. doi: 10.1152/jn.00353.2001, 2002.
[2] Ivorra A., *et al.*, doi: 10.1039/c004419a, 2010.
[3] Mercadal B., *et al*. doi: 10.1007/s00232-016-9907-0, 2016.

NanoediT: nanoneedle-mediated genomic editing for hypoimmunogenic regulatory T cell manufacturing

Ethan Newman[1], Alberto Sanchez-Fueyo[2], Ciro Chiappini[1]; *[1]Faculty of Dentistry, Oral & Craniofacial Sciences, Centre for Craniofacial & Regenerative Biology, King's College London, Guy's Tower, London, UNITED KINGDOM; [2]Faculty of Life Sciences & Medicine, Institute of Liver Studies, King's College London, London, UNITED KINGDOM*

INTRODUCTION

Regulatory T cells (Tregs) are immune cells that suppress harmful inflammation and equipping them with a synthetic chimeric antigen receptor (CAR) creates a promising therapy for autoimmune disease and transplant rejection. However, each round of CAR-Treg treatment must currently be manufactured bespoke for the individual patient, a process that is both costly and logistically demanding, limiting its wider application.

Generating universal Tregs from healthy donors that could be administered allogeneically rather than autologously would overcome this barrier [1]. Achieving this requires editing the Tregs to prevent rejection, which demands precise multiplex genome engineering, a task that existing delivery systems such as viral vectors, conventional electroporation and nanoparticles cannot adequately perform, owing to poor efficiency, limited payload capacity and toxicity to primary Tregs [2,3].

NanoediT addresses this gap. The platform uses gold-plated nanoneedles on the electrode surface to focus low-power electrical pulses, creating nanoscale membrane pores for intracellular delivery. This approach has been shown to improve delivery efficiency and cell viability over established methods [3], while remaining gentle enough to preserve Treg phenotype. These properties make NanoediT well suited not only to the multiplex genome editing required to render Tregs hypoimmunogenic, but also to delivering the CAR and HLA-E constructs needed for antigen-specific function and NK evasion. Scaling this single-platform approach could make CAR-Treg therapies more accessible and cost-effective.

OBJECTIVE

This project will demonstrate that NanoediT can generate hypoimmunogenic CAR-Tregs by base editing splice sites in the TCR and MHC class I/II genes, delivering an HLA-A2-specific CAR and HLA-E in parallel to prevent NK-mediated clearance.

AIM 1: Engineering multiplex-edited hypoimmunogenic CAR-Tregs using nanoinjection

SpliceR will be used to design sgRNAs targeting conserved splice donor and acceptor sites for base editing of TRAC, B2M and CIITA. Nanoinjection will deliver the editing components intracellularly, with Sanger sequencing used to assess editing outcomes and flow cytometry used to assess phenotype and viability, guiding optimisation of the editing strategy and nanoinjection parameters.

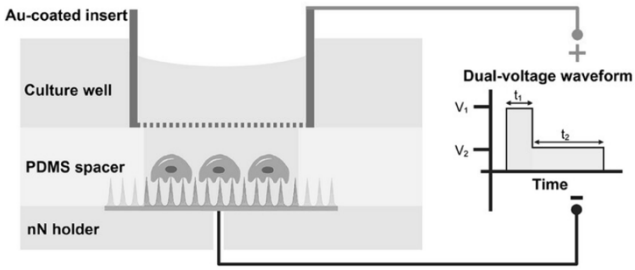
AIM 2: Assess preserved phenotype, suppressive capacity and safety

Simultaneous and sequential editing strategies will be compared to identify the optimal approach to multiplex editing. On-target efficiency and off-target or structural alterations will be quantified by next-generation sequencing, while bulk RNA-seq will confirm elimination of the target transcripts and screen for aberrant splicing or pathway-level changes. Flow cytometry will confirm Treg identity, and edited Tregs will be enriched by bead-based depletion of TCRαβ and MHC I/II, with enrichment efficiency and specificity assessed to establish a GMP-compatible workflow.

AIM 3: Determining hypoimmunogenicity and antigen-specific functionality

Suppressive capacity and CAR functionality will be assessed by co-culturing edited Tregs with HLA-A2$^{+/-}$ antigen-presenting cells and effector T cells, using proliferation and cytokine output as readouts. Co-culture with allogeneic HLA-A2+ PBMCs will assess Treg survival and host CD4+/CD8+ T-cell activation, while co-culture with NK cells will determine susceptibility to NK-mediated clearance using viability, degranulation and cytokine readouts.

Figure 1: Schematic diagram of nanoinjection device. Adapted from [3].



REFERENCES

[1] McCallion O., *et al.* HLA matching or CRISPR editing of HLA class I/II enables engraftment and effective function of allogeneic human regulatory T cell therapy in a humanized mouse transplantation model. *Nat Commun*, 16:9090, 2025.

[2] Napoleone A., *et al.* Overcoming lentiviral delivery limitations in hard-to-transduce suspension cells for genome-wide CRISPR screening. *Mol Ther Adv*, 12;34, 2026.

[3] Sun N., *et al.* Nanoneedle-based electroporation for efficient manufacturing of human primary chimeric antigen receptor regulatory T-cells. *Adv Sci*, 12:2416066, 2025.

Beyond bleomycin: alternative drugs for electrochemotherapy, a review

Evrim Egeden[1], Lora Koenhemsi[2]; *1Kumada Veterinary Polyclinic, Istanbul, TURKEY;*
[2]Department of Internal Medicine, Faculty of Veterinary Medicine, Istanbul University-Cerrahpaşa, Avcılar, 34320 Istanbul, TURKEY

INTRODUCTION

Electrochemotherapy (ECT) relies on passive diffusion of drugs through transient membrane pores. A good ECT drug is too large or too hydrophilic to enter cells on its own, yet small enough to pass through the pores [1]. Bleomycin fits this best: its cytotoxicity rises by more than three orders of magnitude after pulses, so it became the gold standard. Cisplatin is smaller and gains less (about 80-fold). The ESOPE procedures are based on these two drugs only [1]. Drug choice in ECT is therefore narrow, while tumours differ in drug sensitivity and multidrug resistance remains a problem [1]. The aim of this review is to summarise which other agents have been tested with electroporation (EP), with a focus on dogs and cats.

METHODS

A recent review of cytotoxic agents for ECT [1] and veterinary clinical reports on alternative agents [2-5] were reviewed. A good ECT drug was defined by six features: high intracellular cytotoxicity, low permeability without pulses, accumulation in the tumour, low systemic toxicity at ECT doses, clear synergy with EP and immune stimulation [1].

RESULTS

Gain with EP. Most alternative agents gain little from EP; calcium is the exception (Table 1).

Table 1: Fold increase in cytotoxicity with EP [1]. Grey rows: standard ECT drugs.

Agent	Type	Gain with EP
Bleomycin	Hydrophilic	30–5000×
Cisplatin	Hydrophilic	≈80×
Calcium ($CaCl_2$)	Hydrophilic	< 100×
Oxaliplatin	Hydrophobic	2–10×
Mitomycin C	Hydrophilic	≈1.3–1.4×
5-Fluorouracil	Hydrophilic	≈1.25×
Vinblastine	Hydrophobic	1–1.3×
Doxorubicin	Less hydrophilic	≈0.67×
Paclitaxel	Hydrophobic	No increase

Calcium electroporation. Calcium is not toxic by itself. After pulses, Ca^{2+} floods the cell, mitochondria fail, ATP is depleted and the cell dies by necrosis or apoptosis. It is already used in human clinics and may overcome multidrug resistance and trigger immunogenic effects [1].

Veterinary evidence. In three cats with basal cell tumours of the nasal planum, intravenous bleomycin was combined with intralesional $CaCl_2$ (10 mg/mL, ≤1 mg/kg); cisplatin was added in one cat [2]. After one or two sessions 6 weeks apart, all three cats had a complete response, with a local disease-free interval of 9–12 months. Toxicity was grade 2–3 (scabs, nasal discharge, sneezing, transient inappetence). In a cat with melanoma lymph node metastases that recurred 120 days after bleomycin ECT, intravenous bleomycin with intranodal calcium gluconate (9 mM; 8 × 100 µs, 1000 V/cm) gave complete remission of both nodes at 28 days, a disease-free interval of 5 months and survival of 9 months, with only mild, transient oedema and ulceration [3]. In horses, calcium alone (220 mM $CaCl_2$ intratumorally; 8 × 100 µs, 1000 V/cm) gave an objective response in 44% of 27 sarcoids (complete 22%, partial 22%); it was safe and feasible but not yet an alternative to surgery [4]. In a dog with stage IV oral melanoma, calcium added to ECT gave a partial response at 1 month [5].

Other agents. With EP, mitomycin C was more effective than chemotherapy alone in a bladder cancer model, with tumour shrinkage in vivo. Oxaliplatin induced immunogenic cell death at rates similar to other ECT drugs. Doxorubicin uptake was higher in myeloma-bearing mice. In conjunctival melanoma cells, 5-fluorouracil and mitomycin C showed no significant gain, while bleomycin worked [1]. In dogs with head and neck tumours, gemcitabine was used intratumorally when the outcome with bleomycin was unfavourable, but bleomycin remained the preferred agent [5]. Zn(II) complexes, curcumin, glutathione, betulinic acid and vinorelbine are still experimental [1].

Candidates not yet tested. Poorly permeant agents proposed for ECT include mithramycin, daunorubicin, the targeted drugs sotorasib, belzutifan, vemurafenib and sunitinib (vemurafenib showed synergy with bleomycin ECT), and the natural compounds withaferin A and cannabidiol [1].

CONCLUSIONS

Bleomycin is still the gold standard; no alternative comes close to its gain with EP. Calcium is the most practical alternative: it is cheap, not chemotoxic and already works in cats and horses. Other drugs gain little or remain in vitro. New poorly permeant candidates need veterinary trials.

REFERENCES

[1] Morozas A., *et al.* Cytotoxic agents for electrochemotherapy: efficacy, mechanisms of action, potential candidates. *Biomed Pharmacother*, 191:118451, 2025.
[2] Salmoral A., *et al.* Electrochemotherapy for the treatment of basal cell tumours of the nasal planum in three cats. *JFMS Open Rep*, 10, 2024.
[3] dos Anjos D. S., *et al.* Electrochemotherapy associated with calcium electroporation in metastatic feline cutaneous malignant melanoma. *Acta Sci Vet*, 47, 2019.
[4] Frandsen S. K., *et al.* Calcium electroporation of equine sarcoids. *Animals*, 10:517, 2020.
[5] Nemec A., *et al.* Electroporation-based treatments in small animal veterinary oral and maxillofacial oncology. *Front Vet Sci*, 7:575911, 2020.

Cell-specific responses to patterned bipolar pulses for gene electrotransfer

Alexia Cash[1,4,5], Robert Williamson[1,4,5], Driss Elhanafi[2,4], Michael Sano[3,4]; *[1]Lampe Joint Department of Biomedical Engineering; [2]BTEC College of Engineering; [3]Department of Molecular and Biomedical Sciences; [4]North Carolina State University; [5]University of North Carolina at Chapel Hill, USA*

INTRODUCTION

Gene electrotransfer (GET) is a nonviral method for delivering plasmid DNA into cells using pulsed electric fields [1]. Although conventional monopolar protocols can achieve high transfection efficiencies, relatively long pulses may produce undesirable muscle stimulation and pain during in vivo treatment [2,3]. Bipolar microsecond pulses may reduce these effects while maintaining effective DNA delivery [4]. However, electroporation thresholds and transfection outcomes are strongly dependent on cell type [5]. This study compared GET using patterned bipolar waveforms in "easy to transfect" HEK293 cells and more difficult-to-transfect C28 chondrocytes. Monopolar treatments will be compared to patterned bipolar REVAAMP pulses [1] We hypothesized that waveform performance would differ between the two cell types and that protocols optimized in HEK293 cells would not necessarily produce equivalent outcomes in C28 cells.

METHODS

HEK293 cells were used to optimize electric field intensity and plasmid concentration for conventional monopolar and patterned bipolar microsecond protocols. The highest-performing conventional protocol, 8 × 100 µs, was compared with three bipolar protocols: 2-1-1 unbalanced, 1-1-0.5 unbalanced, and 2-1-1 burst-balanced. Cells were cotransfected with GFPx and RFPx plasmids using cuvette-based electroporation. GET efficiency was calculated as the percentage of viable cells multiplied by the percentage of fluorescent cells [1]. The same optimized protocols and electric field intensities identified using HEK293 cells were subsequently evaluated in C28 chondrocytes. GFP and RFP expression were quantified using flow cytometry 24 h after treatment.

RESULTS AND FIGURES

The optimal protocols differed substantially between the two cell types **(Figure 1)**. In HEK293 cells, the conventional 8 × 100 µs protocol produced the highest total GET efficiency at 67.79 ± 1.25%. The 2-1-1 unbalanced, 2-1-1 burst-balanced, and 1-1-0.5 unbalanced protocols produced GET efficiencies of 58.23 ± 2.14%, 40.08 ± 1.66%, and 38.62 ± 1.05%, respectively [1]. More than 94% of transfected HEK293 cells expressed both plasmids, demonstrating efficient cotransfection. The 1-1-0.5 unbalanced protocol produced the highest median fluorescence intensity despite having lower overall GET efficiency **(Figure 1)** [1]. C28 chondrocytes showed markedly lower GET efficiencies under the same treatment conditions. In contrast to HEK293 cells, the 2-1-1 burst-balanced protocol produced the highest C28 GET efficiency at 16.25 ± 1.94%, exceeding the 8 × 100 µs protocol at 11.63 ± 0.35% [1]. The 2-1-1 unbalanced and 1-1-0.5 unbalanced protocols produced lower efficiencies of 6.50 ± 0.94% and 5.23 ± 0.91%, respectively [1]. Unlike HEK293 cells, most transfected C28 cells expressed only GFPx rather than both plasmids. RFP expression was substantially lower in C28 cells, with median RFP fluorescence approximately one order of magnitude lower than in HEK293 cells [1]. This reduced performance is consistent with the known difficulty of transfecting chondrocytes using nonviral methods [6].

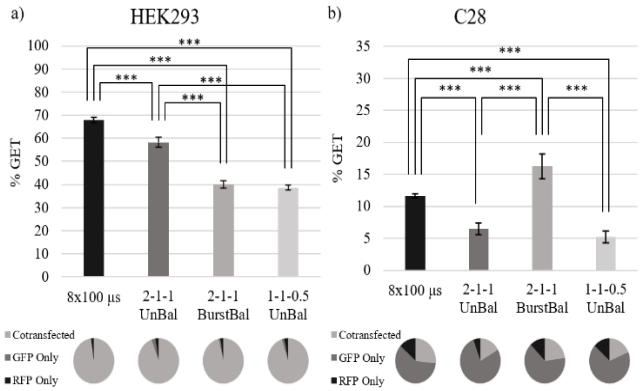


Figure 1: Overall GET efficiency varied significantly between all four protocols tested. Pie charts below each bar represent distribution of cells which were cotransfected, transfected with only GFPx, or (transfected with only RFPx for each respective protocol. Error bars represent one standard deviation from the mean. Significant differences are denoted as * ($p < 0.05$), ** ($p < 0.01$) and *** ($p < 0.001$).

CONCLUSIONS

The conventional 8 × 100 µs protocol was optimal for HEK293 cells. However, the 2-1-1 burst-balanced waveform was the most effective protocol tested in C28 cells and outperformed the conventional protocol in this difficult-to-transfect cell line [1]. These findings demonstrate that GET parameters optimized in HEK293 cells cannot be assumed to translate directly to other cell types. Cell-specific optimization of waveform structure, electric field intensity, plasmid concentration, and delivery conditions will be necessary for reliable application of patterned bipolar pulses to primary or therapeutically relevant cells.

REFERENCES

[1]Cash A. K., *et al.*, doi:10.1007/s10439-026-04106-9, 2026.
[2] Fusco R., *et al.*, doi: 10.5306/wjco.v12.i5.367, 2021.
[3] Cvetkoska A., *et al.*, doi.org/10.1038/s41598-022-12112-9, 2022.
[4] Sano M. B., *et al.*, doi.org/10.1038/srep40747, 2017.
[5] Potočnik T., *et al.*, doi.org/10.3390/app12168237, 2022.
[6] Welter J.F., *et al.* In:Cartilage and Osteoarthritis:Cellular and Molecular Tools. Humana Press, 2004.

Charge-neutral bursts of asymmetric microsecond pulses for in vivo DNA delivery

Robert H. Williamson[1], Michael B. Sano[2]; *[1]Lampe Joint Dep. of Biomed. Eng., North Carolina State University, Raleigh, USA; [2]Dep. of Mol. Biomed. Sci., North Carolina State University, Raleigh, USA*

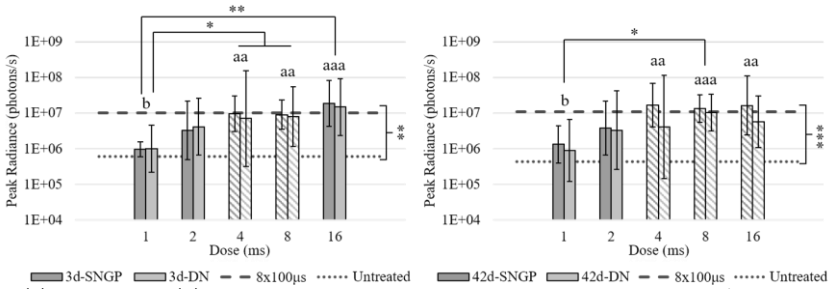


Figure 1: Peak radiances (a) 3-days and (b) 42-days post-treatment. Significance denoted as *p<0.05, **p<0.01, ***p<0.001. Protocols which significantly differed from untreated or conventional GET (8x100µs) denoted with "a" or "b", respectively. Other comparisons denoted with "*". Striped columns are statistically equivalent to conventional GET according to TOST with a meaningful difference of 10% of the conventional GET radiance value (α=0.05).

INTRODUCTION

Reversible electroporation (RE) uses pulsed electric fields to induce temporary nanoscale defects which permeabilize the cell membrane to normally impermeable macromolecules [1]. RE has been used to greatly enhance DNA uptake in vivo in a process referred to as gene electrotransfer (GET). However, conventional GET uses monopolar pulses on the order of 100µs-20ms, which induce intense muscle stimulation and pain in vivo [2-4], limiting clinical utility in DNA vaccine applications.

Ultrashort (<2µs) bipolar pulses can eliminate this muscle stimulation in vivo when used for non-GET related applications such as tissue ablation [2] but require higher DNA concentrations to achieve efficiencies similar to conventional GET due to decreased electrophoretic effects resulting from using symmetrical pulses [5]. However, it has been shown in vitro that asymmetrical bipolar pulses can be arranged into charge-balanced bursts which enable efficiencies similar to conventional GET without higher DNA concentrations [6]. We termed this process Reversible Electroporation Via Algorithmically Mediated Microsecond Pulses (REVAMMP) and, in this study, compare protein expression following GET using REVAMMP to conventional GET in vivo.

METHODS

Healthy BALB/c mice received two GET treatments- one in each gastrocnemius. One used a dual-needle (DN) electrode geometry, and the other used a single needle and grounding pad (SNGP) geometry which utilized the needle of the plasmid injection syringe as the single needle electrode. For each treatment, mice received an intramuscular injection of plasmid DNA followed by GET using either a conventional GET protocol (8x100µs monopolar pulses, 1Hz) or REVAMMP protocol with a dose (integrated on-time) of 1ms, 2ms, 4ms, 8ms, or 16ms delivered at 250V. AkaLuc expression was measured 3-, 7-, 14-, 21-, 28- and 42-days post-treatment using an in vivo bioluminescence imaging system. Peak photon emission (radiance) was calculated and used to compare AkaLuc expression between groups.

Peak radiances for each treatment-applicator pair (n=6) were log-transformed and significant differences determined using a two-way ANOVA followed by Tukey's HSD. Statistical equivalence between groups was tested using TOST. All analyses were performed in JMP Student Edition 19.

RESULTS

AkaLuc expression was achieved in all GET groups and remained stable until the 42-day timepoint. Peak radiance values did not differ significantly between applicators, though the SNGP groups tended to have lower standard deviations than DN groups.

At the 3-day timepoint, peak radiance values for the 4ms, 8ms and 16ms REVAMMP protocols were significantly higher than the untreated control and 1ms REVAMMP protocol. The 4ms and 8ms REVAMMP protocols were statistically equivalent to the conventional protocol. The 16ms REVAMMP group had a higher peak radiance than the conventional protocol, however these groups were neither statistically equivalent nor different.

At the 42-day timepoint, peak radiance values for the 4ms, 8ms and 16ms REVAMMP protocols were significantly higher than the untreated control and statistically equivalent to the conventional monopolar protocol.

CONCLUSIONS

REVAMMP protocols can achieve durable protein expression at levels equivalent to conventional RE with potential to reduce muscle stimulation in a clinical setting. However, the REVAMMP waveform used in this study requires much higher doses (integrated on-time) to do so. A more optimal REVAMMP waveform may allow for a reduction in dose. For example, parameters such as intra- and inter-burst frequency have been proposed to affect GET [7] and could be used to improve REVAMMP outcomes. Thus, further investigation into the REVAMMP parameter space is warranted.

REFERENCES

[1] doi: 10.3390/ijms20112776
[2] doi: 10.1088/1361-6560/aa8c53
[3] doi: 10.5306/wjco.v12.i5.367
[4] doi.org/10.1038/s41598-022-12112-9
[5] doi.org/10.3390/app12168237
[6] doi.org/10.1007/s10439-026-04106-9
[7] doi: 10.1109/TDEI.2018.007777.

Response of patient-derived glioblastoma stem and differentiated cell spheroids to high-frequency biphasic electric pulses

Matej Turk[1], Anja Blažič[1], Zala Vidic[1], Bernarda Majc[2], Klara Bulc Rozman[1], Metka Novak[2,3], Barbara Breznik Vittori[2,4], Lea Rems Mahnič[1]; *[1]University of Ljubljana, Faculty of Electrical Engineering, Ljubljana, SLOVENIA; [2]National Institute of Biology, Ljubljana, SLOVENIA; [3]University of Ljubljana, Biotechnical Faculty, Ljubljana, SLOVENIA; [4]University of Ljubljana, Faculty of Chemistry and Chemical Technology, Ljubljana, SLOVENIA*

INTRODUCTION

Glioblastoma (GB) is a highly aggressive brain tumor characterized by profound cellular heterogeneity, including glioblastoma stem cells (GSCs) [1]. High-frequency irreversible electroporation (H-FIRE) is being investigated as a local treatment approach for brain tumors [2], but differences in treatment sensitivity between stem and differentiated cells remain insufficiently understood. Spheroids formed from patient-derived GB cells provide a 3D model for examining these differences [3]. This study compared cell membrane permeabilization and cell survival (assessed by metabolic activity and viable cell count) in GSC and matched differentiated cell spheroids exposed to high-frequency biphasic electric pulses, while examining spheroid size, electric field distribution, medium conductivity and sample heating.

METHODS

Spheroids were prepared from GSCs and matched differentiated GB cells obtained from three patients (NIB216, NIB225, NIB237). Spheroid size was measured by brightfield microscopy. Numerical modeling evaluated how spheroid size and position affected electric field distribution within the cuvette. Spheroids were exposed in 4 mm cuvettes to 100 trains of 25 biphasic pulses (2–5–2–5 µs, repetition rate 1 Hz) at fields up to 2.5 kV/cm. Membrane permeabilization was assessed by propidium iodide (PI) staining and flow cytometry. Cell survival was evaluated 24 hours after treatment using the CellTiter-Glo 3D metabolic assay (Promega) and direct counting of viable cells using Trypan blue. Current, voltage, and temperature changes were recorded during pulse delivery.

RESULTS AND FIGURES

Increasing electric field strength enhanced membrane permeabilization and reduced metabolic activity (Fig. 1). However, in differentiated spheroids, the low CellTiter-Glo 3D signals disagreed with their preserved compact structure. This assay measures ATP released through cell lysis; additional assay based on counting viable cells at 24 hours, following spheroid dissociation, confirmed that differentiated cell spheroids were incompletely lysed. The cell counting assay showed greater sensitivity of GSCs than their matched differentiated counterparts in NIB216 and NIB237.

GSCs formed larger spheroids than differentiated cells, but numerical modeling showed only a minor effect of spheroid size on the local electric field, with spheroid position having a greater influence. Size alone therefore did not explain the observed response differences, while the more compact organization of differentiated spheroids might contribute to their lower sensitivity. Differences in exposure conditions were also observed: higher conductivity of the differentiated cell medium was accompanied by higher currents and greater heating (Table 1), with the temperature reaching approximately 68.2 °C at 1000 V. Despite greater heating, differentiated cells remained less sensitive, indicating that thermal effects alone cannot explain the differences between phenotypes.

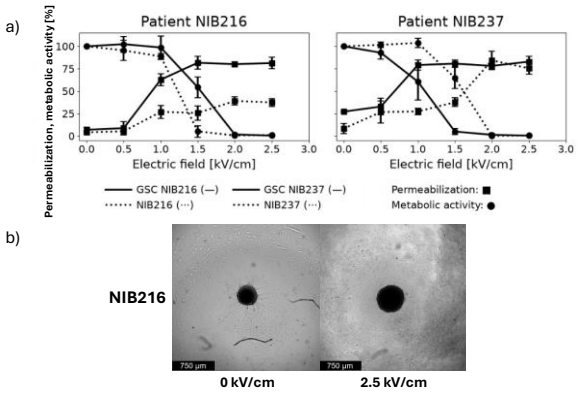


Figure 1: a) Percentage of permeabilized cells (squares) and metabolic activity (circles) 24 hours post-electroporation as a function of electric field strength in GSC (solid lines) and differentiated cell spheroids (dashed lines) ($N = 3$). b) Representative micrographs of NIB216 cell spheroids 7 days post-electroporation, showing control (0 kV/cm, left) and treated spheroid (2.5 kV/cm, right).

Table 1: Relative current changes (ΔI) and temperature increases (ΔT) in growth media used for electroporation.

Growth medium	U[V]	ΔI[%]	ΔT[°C]
Diff. cells	600	7.3	8.8
Diff. cells	1000	47.0	32.2
GSC	600	16.6	5.1
GSC	1000	32.3	16.3

CONCLUSION

GSC spheroids were more sensitive to electroporation than matched differentiated spheroids under the tested conditions. These findings highlight the importance of exposure conditions and survival assessment, while the role of spheroid compactness will be explored further.

REFERENCES

[1] Obrador E., *et al.*, doi: 10.3390/ijms25052529, 2024.
[2] Latouche E. L., *et al.*, doi: 10.1177/1533033818785285, 2018.
[3] Ivey J. W., *et al.*, doi: 10.34133/2019/8081315, 2019.

In silico modeling of multicellular tumor spheroids for the optimization of DNA vaccine electroporation

Léa Joseph[1], Clair Poignard[1], Annabelle Collin[2], Stéphane Urcun[1], Juliette Codevelle[1,3], Charlotte Rivière[3,4,5] and Estelle Bastien[3]; *[1]AIMOKA: INRIA, Assistance Publique-Hôpitaux de Paris, Université Sorbonne Paris Nord, Rennes, FRANCE; [2]Laboratoire de Mathématiques Jean Leray, Nantes Université, FRANCE; [3]Université Lyon 1, CNRS UMR5306, Institut Lumière Matière, Villeurbanne, FRANCE; [4]Université de Lyon 1, INSERM U1052-CNRS UMR5286, Centre Léon Bérard, Centre de Recherche en Cancérologie de Lyon, Plateforme μfab, Institut Convergence Plascan, Lyon, FRANCE; [5]Institut Universitaire de France (IUF), FRANCE*

INTRODUCTION

DNA vaccination via Electroporation (EP) is a promising approach for next-generation therapies, particularly in hepatocellular carcinoma (HCC). However, its physical basis remains poorly understood and current vaccination protocols are empirical and non-personalized. Our upcoming PhD project VAPHOC focuses on the mathematical modelling of DNA vaccination based on experimental data. This builds upon our previous work on multicellular tumor spheroids, where we modelled the structural mechanisms of tumor adaptability under nutritional stress.

METHODS

We previously developed a macroscopic growth model based on Ordinary Differential Equations (ODEs) calibrated with the SAEM algorithm, alongside a spatially resolved Agent-Based Model (Cellular Potts Model). For the VAPHOC project, a complete Multiphysics and multiscale framework will be constructed. A poroelastic spheroid model [1] will be developed to quantify DNA plasmid distribution in relation to the secreted extracellular matrix (ECM). DNA entry into cells via EP will then be modelled by describing the electric field within the spheroid.

PRELIMINARY RESULTS

Preliminary results from the master's thesis demonstrated that the intrinsic growth rate and critical environmental threshold are invariant properties of the HCT116 cell line under metabolic stress. The mathematical model successfully uncoupled protocol specific artifacts from intrinsic biological dynamics.
For the upcoming electroporation phase, the primary novelty of this research lies in performing a tumor-specific optimization of electric pulse parameters (High short Voltage-Low long Voltage) [2]. For the first time as our knowledge, this numerical optimization will explicitly integrate the density of the ECM. Advanced computational strategies, such as kriging numerical optimization, will be used to explore parameter spaces and maximize DNA cellular uptake by linking spheroid porosity, extracellular DNA distribution and cell transfection.

CONCLUSIONS

Bridging varied modelling scales, from single-cell metabolic adaptation to continuous spatial Partial Differential Equations (PDEs), lays a groundwork for developing integrated predictive numerical tools. Ultimately, this research aims to design numerically optimized, ECM-specific electroporation protocols to improve the efficacy and reliability of therapeutic DNA transfer.

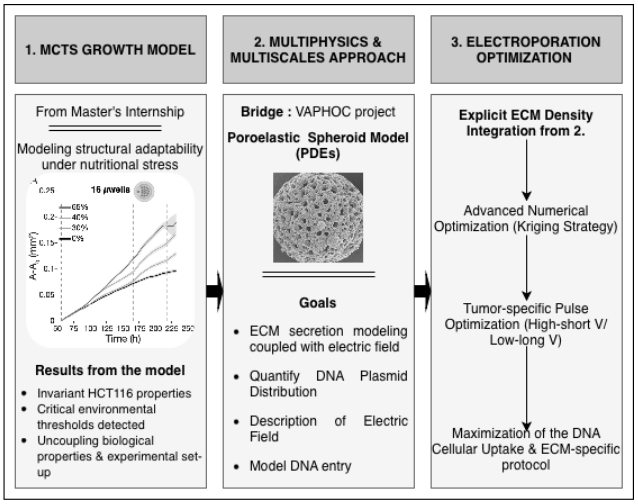


Figure 1: Conceptual framework of the VAPHOC project: bridging macroscopic spheroid growth models with poroelastic extracellular matrix dynamics to optimize DNA electroporation.

REFERENCES

[1] Urcun S., *et al*. Digital twinning of cellular capsule technology: Emerging outcomes from the perspective of porous media mechanics. *PLOS ONE*, 16:1-30, 2021.
[2] André F. M., *et al*. Efficiency of high and low-voltage pulse combinations for gene electrotransfer in muscle, liver, tumor, and skin. *Hum Gene Ther*, 19:1261-71, 2008.

Calcium-dependent electroporation responses: cytotoxicity, tumor suppression and annexin A4 membrane repair

Lukas Giedrimas[1], Baltramiejus Jakštys[1], Paulius Ruzgys[1], Renaldas Raišutis[2,3], Saulius Šatkauskas[1], Martynas Maciulevičius[1,2]; *[1]Research Institute of Natural and Technological Sciences, Vytautas Magnus University, LITHUANIA; [2]Ultrasound Research Institute, Kaunas University of Technology, LITHUANIA; [3]Department of Electrical Power Systems, Faculty of Electrical and Electronics Engineering, Kaunas University of Technology, LITHUANIA.*

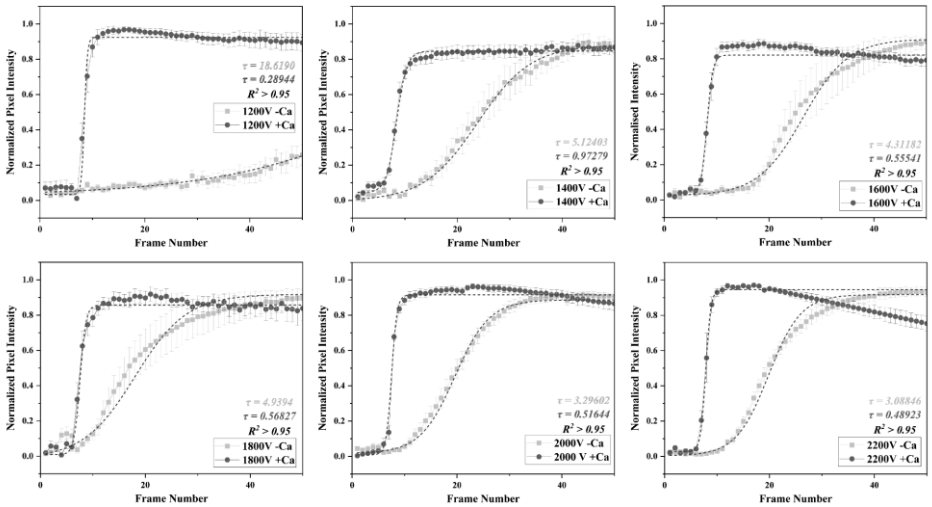


Figure 1: Paired normalized ANXA4 fluorescence kinetics with (+Ca^{2+}) and without (−Ca^{2+}) extracellular calcium at 1.2–2.2 kV/cm; dashed lines show fitted response curves ($R^2 > 0.95$).

INTRODUCTION

Electroporation (EP) transiently permeabilizes the plasma membrane, enabling uptake of ions and cytotoxic agents. Calcium electroporation (Ca^{2+} EP) is being investigated as an alternative to drug-based electrochemotherapy [1]. Ca^{2+} influx can drive cytotoxicity while also activating membrane repair. Annexin A4 (ANXA4), a Ca^{2+}- and phospholipid-binding repair protein [2], therefore provides a molecular readout of membrane injury and resealing. We examined complementary Ca^{2+}/bleomycin treatment responses and ANXA4 dynamics after EP.

METHODS

CHO, MX-1 and 4T1 cells received $CaCl_2$ (0–5 mM) or bleomycin (BLM; 1–20 nM) before a single 100 µs pulse (800–1600 V/cm). PI flow cytometry (20 min), MTT (24 h) and clonogenic assay (6 days) assessed treatment response. 4T1 tumors treated with Ca^{2+} EP or BLM electrotransfer were followed for 11 days. Separately, MCF-7 wild-type and ANXA4-knockout cells were electroporated ±5 mM extracellular Ca^{2+} with single 100 µs pulses up to 2.2 kV/cm; paired comparisons used 1.2–2.2 kV/cm. ANXA4-GFP redistribution was quantified from live-cell images using membrane/cytosolic ROIs with Fiji/MATLAB.

RESULTS

Ca^{2+} EP produced earlier cytotoxicity than BLM in CHO and MX-1 cells, whereas 4T1 cells responded early to both treatments. Increasing field strength reduced the agent concentration required for comparable cytotoxicity; in MX-1, the BLM concentration associated with 50% cytotoxicity decreased from approximately 7.15 nM at 800 V/cm to 1.5 nM at 1600 V/cm, with a similar trend in 4T1. Ca^{2+} EP and BLM both markedly suppressed 4T1 tumor growth over 11 days. In the ANXA4 model, extracellular Ca^{2+} induced rapid, stable ANXA4-GFP membrane recruitment, whereas Ca^{2+}-free conditions remained predominantly diffuse/cytosolic. With Ca^{2+} present, higher field strength accelerated recruitment, increased cortical fluorescence and prolonged membrane residency. Recruitment half-times were significantly shorter with extracellular Ca^{2+} (approximately 6–10 versus 18–25 frames; $p < 0.05$; Figure 1). ANXA4-deficient cells showed impaired resealing and reduced survival.

CONCLUSIONS

Ca^{2+} EP combines rapid cytotoxic action with in vivo tumor suppression comparable to BLM, while extracellular Ca^{2+} also activates ANXA4-dependent membrane repair. Thus, electroporation outcome reflects both treatment intensity and the cell's capacity for Ca^{2+}-dependent resealing. These datasets will also guide future Fluorescence Analyzer development for standardized time-resolved single-cell fluorescence analysis.

REFERENCES

[1] Frandsen S. K., *et al.* Direct therapeutic applications of calcium electroporation to effectively induce tumor necrosis. *Cancer Res*, 72:1336–1341, 2012.

[2] Boye T. L., *et al.* Annexin A4 and A6 induce membrane curvature and constriction during cell membrane repair. *Nat Commun,* 8:1623, 2017.

Evaluation of circulating tumor cell dynamics following electroporation or electrochemotherapy in a 4T1 mouse model of metastatic breast cancer

Veronika Škrjanc[1,2], Maja Čemažar[1,2,3], Boštjan Markelc[1,2,4], Simona Kranjc Brezar[1,2], Lucija Kenda[2], Maja Aurora Keber[2], Pia Lara Korošec[2], Gregor Serša[1,2,4], Tanja Jesenko[1,2]; *[1] Institute of Oncology Ljubljana, Zaloška cesta 2, 1000 Ljubljana, SLOVENIA; [2] University of Ljubljana, Faculty of Medicine, Vrazov trg 2, 1000 Ljubljana, SLOVENIA; [3] University of Primorska, Faculty of Health Sciences, Polje 42, 6310 Izola, SLOVENIA; [4] University of Ljubljana, Biotechnical Faculty, Jamnikarjeva ulica 101, 1000 Ljubljana, SLOVENIA*

INTRODUCTION

In advanced breast cancer, electrochemotherapy (ECT) is an effective local treatment for cutaneous metastases that combines the administration of cytotoxic drugs with the delivery of electric pulses to the tumour. The electric pulses transiently increase the permeability of tumour-cell plasma membranes, thereby facilitating intracellular drug uptake and enhancing cytotoxic efficacy [1]. In addition to electroporation of tumour cells, ECT induces changes in the tumour vasculature, including vascular lock, disruption of intercellular contacts and increased vascular permeability. Although these effects contribute to enhanced drug accumulation within the tumour, the temporary loss of vascular integrity and separation of endothelial cells could theoretically facilitate the entry of tumour cells into the systemic circulation [2]. This raises the possibility that ECT may influence the release of circulating tumour cells (CTCs) and potentially affect tumour dissemination, as has also been demonstrated for other vascular-disrupting therapies. However, the effect of ECT on CTC release has not yet been experimentally evaluated.

AIM

The aim of this study was to evaluate ECT's impact on the number and temporal dynamics of CTCs in a 4T1 metastatic breast cancer mouse model, to verify whether vascular changes increase tumour cell release.

METHODS

The study was conducted using the 4T1 triple-negative breast cancer mouse model. Mice were allocated to three experimental groups: untreated control (CTRL), electroporation alone (EP), and electrochemotherapy (ECT; intravenous bleomycin administered at a dose of 5 mg/kg body weight, followed by electroporation). Terminal blood samples were collected by cardiac puncture at 2 hours, 2 days, or 7 days after treatment. CTCs were enriched using the Parsortix® system (CelLBxHealth plc, UK) and identified using morphological assessment and immunofluorescence staining for Hoechst, pan-cytokeratin, CD45, vimentin, and N-cadherin. Tumour volumes were measured before treatment and at the time of blood collection. Data were analysed using one-way analysis of variance (ANOVA), followed by Tukey's multiple-comparisons test, with $p < 0.05$ considered statistically significant.

RESULTS

ECT induced a pronounced antitumor response, with significantly reduced tumour volumes at 2 and 7 days after treatment. No significant differences in total CTC numbers were observed among the experimental groups at 2 hours or 2 days after treatment (Figure 1). At day 7, however, CTC numbers were significantly lower in ECT group than in the CTRL group (Figure 1). The numbers of mitotic CTCs and CTC clusters did not differ significantly among the groups at any time point.

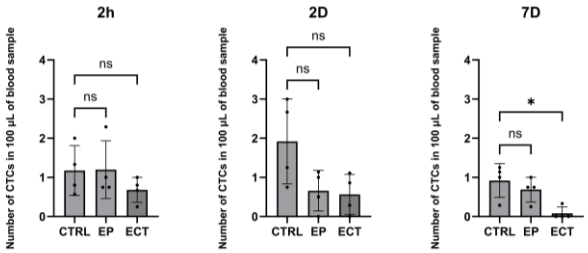


Figure 1: Number of circulating tumour cells (CTCs) following treatment. The number of CTCs detected in 100 µL of blood was determined 2 hours (2h), 2 days (2D), and 7 days (7D) after treatment in the untreated control (CTRL), electroporation (EP), and electrochemotherapy (ECT) groups. Bars represent mean ± SD, and individual data points represent individual samples. Statistical significance is indicated above the brackets: $p < 0.01$; ns, not significant.

CONCLUSIONS

In the 4T1 triple-negative breast cancer mouse model, ECT did not induce a detectable increase in circulating CTC numbers. Instead, CTC numbers were reduced 7 days after treatment, coinciding with a pronounced antitumor response. These findings provide preclinical evidence that the transient vascular changes induced by ECT do not promote the immediate release of tumour cells into the circulation, which confirms the safety of the treatment method.

REFERENCES

[1] Serša G., *et al*. Electrochemotherapy of chest wall breast cancer recurrence. *Cancer Treat Rev*, 38:379–386, 2012.

[2] Pantel K., *et al*. Liquid biopsy and minimal residual disease—latest advances and implications for cure. *Nat Rev Clin Oncol*, 16:409–424, 2019.

Therapeutic role of bleomycin-based electrochemotherapy in the treatment of locally advanced- and recurrent vulva carcinomas

Agnes Simo[1], Erika Kis[1], Gyorgy Lazar[2], Judit Olah[3], Attila Paszt[2], Gabor Vass[1], Ali Mirmohammadsadeghi[1], Petra Rozsa[1], Mario Vincze[4], Norbert Antal[5], Aurel Ottlakan[2];

INTRODUCTION

Vulvar carcinoma (VC) accounts 5% of gynecological malignancies, with incidence increasing with age.[1] Surgical resection remains the standard treatment, but repeated surgical interventions may result in extensive tissue loss, perineal defect, chronic complications, and reduced quality of life (QoL)[2,3]. Electrochemotherapy (ECT) has emerged as a minimally invasive, tissue-sparing local treatment that enhances intracellular drug uptake through reversible electroporation.

OBJECTIVE

This systematic review aimed to evaluate the efficacy of ECT in VC, focusing on tumor response, local symptom control, tissue preservation, and QOL.

METHODS

A systematic literature review was conducted in the period of 1990-2026 according to the PRISMA guidelines to identify studies investigating ECT for VC (Figure 1.) Our search strategies weres as follows: ("vulva"[MeSH Terms] OR "vulva"[All Fields] OR "vulvar"[All Fields]) AND ("carcinoma"[MeSH Terms] OR "carcinoma"[All Fields] OR "carcinomas"[All Fields] OR "carcinoma s"[All Fields]) AND ("electrochemotherapy"[MeSH Terms] OR "electrochemotherapy"[All Fields] OR "electrochemotherapies"[All Fields]) AND "electro-chemotherapy"[All Fields].

RESULTS

Fifteen studies involving 274 patients met our preset inclusion criteria, most of them had SCC, while five had other tumor types. The median follow-up was 8.8 months, showing considerable variability in tumor response: CR 11.1-100%, PR:12,5-66,7%, SD:9,8-100%, PR:5,5-25%. This variability may be attributable to differences in tumor size, disease stage and its characteristics. Six studies reported improved QoL, primarily associated with pain reduction. ECT may also alleviate local symptoms while preserving anatomical structures . However, limited patients number and prior oncological treatments restrict the comparability of outcomes.

CONCLUSION

ECT represents a promising tissue-sparing approach for local tumor control in selected patients with locally advanced or recurrent VC, as a major issue in these patients is the frequent occurrence of urinary incontinence and anal sphincter impairment. Its potential benefits extend beyond tumor reduction to symptom relief and preservation of QoL. Nevertheless, the shortage of clinical evidence highlights the need for prospective studies with standardized response assessment and long-term follow-up to establish its optimal position within multidisciplinary treatment algorithms.

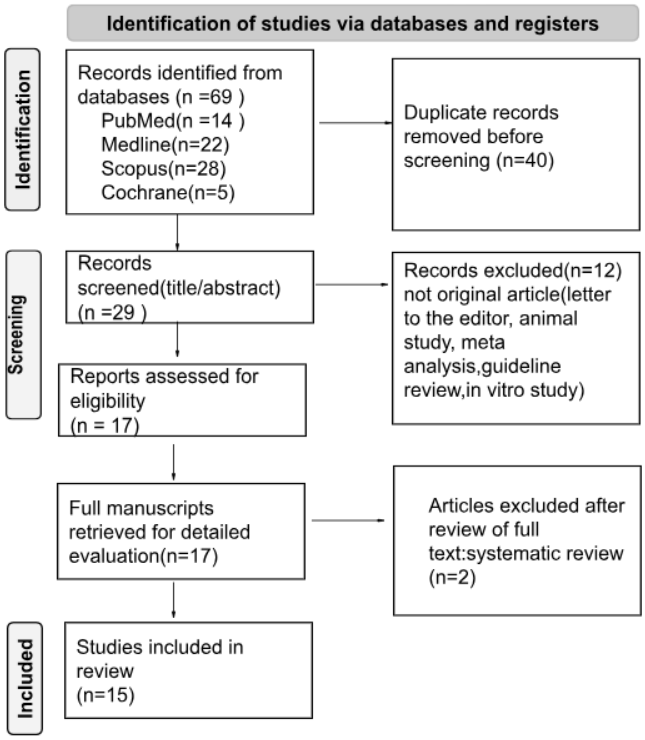


Figure 1: PRISMA flow diagram.

REFERENCES

[1] Darwish A., *et al*. Prognostic characteristics, recurrence patterns, and survival outcomes of vulval squamous cell carcinoma - A twelve-year retrospective analysis of a tertiary centre. *Eur J Surg Oncol*, 50:108447, 2024.

[2] Perrone A. M., *et al*. Quality of life with vulvar carcinoma treated with palliative electrochemotherapy: the ELECHTRA (ELEctroCHemoTherapy vulvaR cAncer) Study. *Cancers (Basel)*, 13:1622, 2021.

[3] Vivod G., *et al*. Quality of life of women with recurrent vulvar cancer treated with electrochemotherapy. *Radiol Oncol*, 59:267-276, 2025.

Electrochemotherapy for the treatment of perianal carcinoma concomitant with cervical cancer

Selva Cuellar[1], Laura Lay[1], Marina R. D. Silva[2], Nazarena S. Martínez[2], Sebastián D. Michinski[3], Marcela Ostojich[1], Felipe H. Maglietti[2]; *[1]Instituto de Oncología A. H Roffo, Universidad de Buenos Aires, ARGENTINA; [2]Instituto Barceló de Investigación Traslacional (InBIT), Fundación H. A. Barceló-CONICET, Buenos Aires, ARGENTINA; [3]Instituto de Física Interdisciplinaria y Aplicada (INFINA), Universidad de Buenos Aires - CONICET, Buenos Aires, ARGENTINA*

INTRODUCTION

Perianal or anal margin carcinoma is a rare malignant neoplasm, accounting for approximately one-quarter to one-third of all cancers of the anal region [1]. The most common type is squamous cell carcinoma (SCC), which is almost always associated with infection by human papillomavirus (HPV) types 16 or 18, considered its etiological agent [2, 3].

The management of perianal malignant neoplasms often involves surgical intervention, with wide local excision being a common approach for localized tumors. In some cases, particularly when surgery is not feasible, alternative treatments such as radiotherapy or chemoradiotherapy may be used [4].

The diagnosis and treatment are challenging, together with the reluctance of many patients to seek medical attention for anorectal discomfort, may lead to misdiagnosis and delays in appropriate treatment. Furthermore, given the complexity and rarity of perianal carcinomas, a multidisciplinary approach is essential to optimize outcomes, highlighting the need for dermatologic surgeons and oncologists to be familiar with the clinical presentation and therapeutic options for these neoplasms [5].

CASE PRESENTATION

An 89-year-old female patient was diagnosed with stage IVA cervical carcinoma with bladder involvement and a concomitant perianal squamous cell carcinoma and perianal lesions, HPV positive. Due to a significant decline in quality of life (Scale ECOG 3), she initiated radiotherapy without chemosensitization. She completed a pelvic radiotherapy regimen of 4600 cGy, resulting in an improved performance status (ECOG 0), although anal lesions persisted. Given this finding, electrochemotherapy was initiated. Two sessions were administered over four months, with minimal adverse effects and no negative impact on the quality of life. The patient achieved a complete response according to RECIST criteria. Nine months post-electrochemotherapy, MRI showed no evidence of distant pelvic disease, locoregional lymphadenopathy, or anorectal, vaginal or perianal involvement.

DISCUSSION

In this report, we present the case of a patient who was successfully treated with radiotherapy for cervical cancer, but whose concomitant perianal lesions did not resolve.

Although the treatment was well tolerated, local adverse effects were observed and were manageable with medication.

Based on our experience with ECT in different cases, we have observed that ulceration and the need for debridement tend to be more common in previously irradiated areas.

In the present case, a complete response was achieved.



Figure 1: A: Before the first electrochemotherapy (ECT) session. B: Eight months after the first ECT session and four months after the second session, complete resolution is observed.



Figure 2: During treatment, application of the electric field using a needle electrode.

REFERENCES

[1] Wietfeldt E., *et al*. Malignancies of the anal margin and perianal skin. *Clin Colon Rectal Surg* , 22:127-35, 2009.

[2] De Sanjosé S., *et al*. HPV in genital cancers (at the exception of cervical cancer) and anal cancers. *Presse Méd*, 43:e423-8, 2014.

[3] Bjørge T., *et al*. Human papillomavirus infection as a risk factor for anal and perianal skin cancer in a prospective study. *Br J Cancer,* 87:61-4, 2002.

[4] Leonard D., *et al*. Neoplasms of anal canal and perianal skin. *Clin Colon Rectal Surg* , 24:54-63, 2011.

[5] Kosche C., *et al*. Perianal malignancies: a review for the dermatologic surgeon. *Dermatol Surg*, 49:914-20, 2023.

Neoadjuvant, ECT-integrated surgery, and adjuvant chemotherapy for canine metastatic mast cell tumor

Weerawut Wanaprasertsak[1], Makasiri Samanukorn[1], Raiwin Jomsatianchai[2], Chalidaporn Kampang[1]; *[1]Vet Care Animal Hospital, Bangkok, THAILAND; [2]Raiwin Animal Hospital, Bangkok, THAILAND*

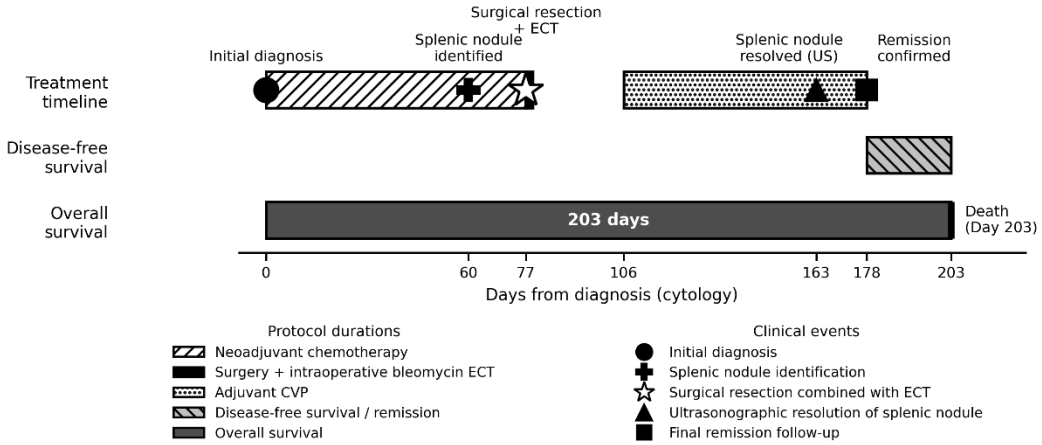


Figure 1: *Monochromatic swimmer plot of the treatment timeline. Bars: white/diagonal (neoadjuvant chemotherapy), black (surgery + intraoperative bleomycin ECT), dotted (adjuvant CVP), gray/diagonal (disease-free survival), dark gray (overall survival, 203 days). Markers: diagnosis (circle), splenic nodule detected (cross), surgery+ECT (star), nodule resolved on US (triangle), final follow-up (square). ECT: unipolar generator (ELECTROvet EZ-V4.0) with a 4-needle array (2×2, 10-mm needles, 3.15-mm tip gap, 4-mm row gap).*

INTRODUCTION

We report a high-grade, metastatic canine mast cell tumor (MCT) treated with neoadjuvant chemotherapy, ECT-integrated surgery, and adjuvant chemotherapy.

CASE PRESENTATION

A 10-year-old male Thai Bangkaew dog (30 kg) presented with a right axillary mass. Cytology revealed necrotic exudate with atypical, degranulated mast cells consistent with MCT; biopsy was withheld due to degranulation risk. Disseminated nodules at presentation indicated Stage 3 disease. Two weekly cycles of vinblastine-prednisolone (VP) produced no response, prompting a switch to cyclophosphamide-vinblastine-prednisolone (CVP). During the first CVP cycle, the dog developed acute hepatitis (ALT >650 U/L) from accidental topical prednisolone ingestion, and ultrasound identified a splenic mass (0.45 × 0.61 cm). During the third cycle, a new preputial mass worsened the prognosis from guarded to poor. After five CVP cycles, the thoracic mass was excised en bloc with intraoperative ECT (IV bleomycin, 15,000 IU/m^2): a needle probe was inserted directly into the exposed fascia to deliver pulses across the tumor bed and a 2-cm margin, sparing the apposed wound edges. Adjuvant CVP resumed four weeks post-surgery.

RESULTS & OUTCOME

The ECT site healed well, with sutures removed on day 10; ECT prevented regrowth of the unresectable mass. Four small skin nodules appeared post-ECT but resolved completely. By the fifth adjuvant cycle, the splenic mass had fully resolved on ultrasound. After six adjuvant cycles, the dog achieved complete clinical remission with no recurrence; renal function stayed stable, and the corticosteroid-induced hepatitis stayed in remission. Side effects were mild, limited to occasional vomiting and low-grade anemia; cachexia, neutropenia, and thrombocytopenia never developed. On day 202, 24 days after remission was confirmed, the dog became acutely lethargic and anorexic with hypotension (56 mmHg) that responded only transiently to fluid boluses, and died on day 203. No necropsy was performed; death is presumed to be mast cell degranulation-related. Overall survival was 203 days from diagnosis (Figure 1).

CONCLUSIONS

In dogs with metastatic MCT, expected median survival without treatment is 1–3 months; this dog survived 203 days. Chemotherapy with ECT-integrated surgery kept local disease controlled for about four months after surgery, and quality of life stayed good until the final day. One case cannot show more, but it may be a reasonable option for metastatic MCT.

REFERENCES

[1] Lowe R., *et al.* The treatment of canine mast cell tumours with electrochemotherapy with or without surgical excision. *Vet Comp Oncol*, 15:252-260, 2017.

[2] Mullins M. N., *et al.* Evaluation of prognostic factors associated with outcome in dogs with stage IV mast cell tumors: 85 cases (1998–2011). *J Am Vet Med Assoc*, 245:800-808, 2014.

[3] Camps-Palau M., *et al.* Treatment of canine mast cell tumours with vinblastine, cyclophosphamide and prednisone: 35 cases (1997-2004). *Vet Comp Oncol*, 5:156-167, 2007.

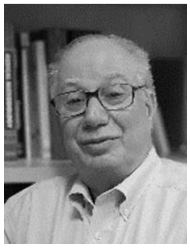
Faculty members



Rafael V. Davalos
Georgia Tech, USA
E-mail:
rafael.davalos@bme.gatech.edu



Julie Gehl
University of Copenhagen, Department of Clinical Medicine, Denmark
E-mail: kgeh@regionsjaelland.dk



Richard Heller
College of Engineering and Morsani College of Medicine, University of South Florida, USA
E-mail:
rheller@usf.edu



Antoni Ivorra
Universitat Pompeu Fabra, Spain
E-mail:
antoni.ivorra@upf.edu



Damijan Miklavčič
University of Ljubljana, Faculty of Electrical Engineering, Slovenia
E-mail: damijan.miklavcic@fe.uni-lj.si



Lluis M. Mir
Université Paris-Saclay, CNRS, France
E-mail:
luis.mir@cnrs.fr



Marie-Pierre Rols
IPBS-CNRS, France
E-mail:
rols@ipbs.fr



Gregor Serša
Institute of Oncology, Slovenia
E-mail:
gsersa@onko-i.si



Mounir Tarek
Theoretical Physics and Chemistry Laboratory, Université de Lorraine, France
E-mail:
mounir.tarek@univ-lorraine.fr



Atul Verma
McGill University, Canada
E-mail:
atul.verma@mcgill.ca



P. Thomas Vernier
Frank Reidy Research Center for Bioelectrics, Old Dominion University, USA
E-mail:
pvernier@odu.edu

Organized by:

UNIVERZA V LJUBLJANI
University of Ljubljana

ONKOLOŠKI INŠTITUT
INSTITUTE OF ONCOLOGY
LJUBLJANA

Supported by:

Abbott

ArgáMedtech
NEXT GENERATION CARDIAC ABLATION

BES
The Bioelectrochemical Society

Boston Scientific

CARDIO FOCUS

COBIK

elea

Field MEDICAL

IGEA
CLINICAL BIOPHYSICS

imricor

ION OPTIX

ISEBTT International Society for Electroporation-Based Technologies and Treatments

IskraMedical

IVY BIOMEDICAL

Johnson&Johnson
MedTech

Kardium

ELECTROvet EZ
by LEROY BIOTECH

LIFE PULSE

Medtronic

MIRAI MEDICAL

mpor

omega

p:o
Clean visions.

Pulse Biosciences

VITAVE

ISBN 978-961-243-506-6

9 789612 435066